NASA TECHNICAL MEMORANDUM

NASA TM X- 72767

COPY NO.

NASA TM X-

EXPERIMENTAL EVALUATION OF TWO 36" x 47" GRAPHITE/EPOXY SANDWICH SHEAR WEBS

By

Harold G. Bush

August 27, 1975

NATIONAL AERONAUTICS AND SPACE ADMINISTRATION

LANGLEY RESEARCH CENTER, HAMPTON, VIRGINIA 23665

EXPERIMENTAL EVALUATION OF TWO 36" x 47" GRAPHITE/EPOXY SANDWICH SHEAR WEBS

By Harold G. Bush
Langley Research Center

INTRODUCTION

The information presented in this report represents initial results of a program initiated at Langley Research Center to study generic structures (i.e.- shear webs, compression panels, etc.) across a wide load range. It is the purpose of this program to identify efficient concepts for each generic structure, and to experimentally establish the performance characteristics of each concept. Particularly, this report details the design and test of two large (36" x 47") graphite-epoxy sandwich shear webs. One sandwich web was designed to exhibit strength failure of the facings. This shear web was identical in size and was designed for the same shear loading as the stiffened, titanium clad boron/epoxy web of reference 1, to provide an alternative concept if desired. The second shear web was the same size but was designed to fail in general instability to identify problem areas of stability critical sandwich webs and to assess the adequacy of contemporary analysis techniques.

TEST COMPONENTS

Two structural shear webs were designed and fabricated for test. The facings of both webs were graphite-epoxy (Thornel 300/Narmco 5208) and the core was aluminum (Hexcel 3/16-5052-.003, ρ = 8.1 pcf). Properties of the graphite-epoxy (Gr/E) used for design are given in Tables 1-3. Table 1 details the lamina elastic properties of T300/5208 while Table 2 itemizes the theoretical, orthotropic average elastic properties of a $(\pm 45°_n)_s$ laminate. Table 3 gives the experimental strengths and elastic properties obtained from tests of sandwich specimens with $(\pm 45°_n)_s$ T300/5208 laminate faces and aluminum H/C core. Details of the material tests listed in Table 3 are given in Appendix A.

Strength Critical Shear Web

One graphite/epoxy sandwich panel was designed to exhibit strength failure of the faces at a shear load of 7638 lb/in, which was the design load for the shear web in reference 1. Using the $\pm$ 45° shear strength allowable of Table III, and a nominal ply thickness of .0055 in/ply, the required face thickness was found to be 12 plies (.066") per face. Using the lamina elastic properties listed in Table II, the buckling load for a sandwich with .066" faces was studied as a function of core thickness. Figure 1 shows the results of these calculations which assumed simple support boundary conditions. Based on these results, a core thickness of .6" was selected to prevent buckling at or below the design load of 7638/in. Also shown in Figure 1 is the buckling load for this web as determined from an initial NASTRAN model of the web and

test frame. Figure 2 shows that the NASTRAN calculated stability mode for this web is asymmetric. The calculations indicate that the frame increased the predicted buckling load from approximately 9500 lb/in (simple support-pure shear load) to approximately 11,700 lb/in for the test web.

The final panel design details for the strength critical web are shown in Figure 3 where the bolting arrangement and doubler area design are illustrated. A psuedo-isotropic pattern ($0°/\pm 45°/90°$) was used in the doubler area. Results of laminate bearing and free hole stress concentration tests for the doubler material are detailed in Appendix A. The doubler area was molded integral with the skins which were secondarily bonded to the core with Hysol EA-951 adhesive.

Stability Critical Shear Web

Since the literature is practically devoid of data on structural buckling tests of composite sandwich shear webs, a second graphite epoxy sandwich was designed to be stability critical at a shear load of 5000 lb/in. The purpose of this web was to identify problem areas for sandwich shear webs which are stability critical, and to assess the adequacy of current analytical tools for predicting shear buckling.

A facing thickness of 10 plies (.055") was found to provide an adequate strength margin (approximately 30% at a shear load of 5000 lb/in. Buckling calculations were performed using both NASTRAN and the code of reference 2 for a Gr/E sandwich with .055" faces and various core thicknesses. The results of these calculations are presented in figure 4. As shown in figure 4, the NASTRAN results indicate that a core thickness of 0.375" would result in a critical load of 5000 lb/in. NASTRAN stability mode plots for core thicknesses

less than and greater than .375" were found to be asymmetric (similar to figure 2, therefore, it was anticipated that if linear, elastic buckling occurred, the buckling mode should be asymmetric for a core thickness equal to .375".

The final panel design details for the stability critical shear web are shown in figure 5. With the exception of laminate and core thicknesses, all details of this web are identical to the strength critical web shown in figure 3.

Shear Web Test Frame

The method selected for test of the shear webs is shown in figure 6 and is essentially the same design as was used in reference 1. The test frame consists of a deep beam with built-up aluminum caps. One half of the beam web is a conservatively designed, stiffened aluminum plate as shown in figure 6. The test web and stiffened aluminum web are bolted to aluminum angles which are bolted to the beam caps. Figure 7 shows a graphite/epoxy sandwich installed in the test frame, before it is installed in the test machine. A consequence of this test method is that the specimen is subjected to inplane bending stresses in addition to the desired shear stress. Based on preliminary design, the magnitude of these bending stresses is anticipated to be approximately 10-15% of the shear stress magnitude.

Sandwich Fabrication and Quality Control

The shear web facings were individually molded, vacuum bagged and autoclave cured at 350° F. After cure, each facing was subjected to a C-scan to locate defective laminate areas. The aluminum H/C core edge was filled as shown in figures 3 and 5. The complete sandwich was assembled, bagged and both facings were simultaneously bonded to the core with Hysol

EA-951 adhesive in an autoclave. Each side of the bonded panel was C-scanned in an effort to identify defective bond areas.

After installation in their respective test frames, each shear web was surveyed to determine any pre-test out-of-plane deformations present. Both webs were found to deviate from the flat conditions by approximately the same amount (.012" to .020") in the center region of the test section. The periphery of each test panel was essentially flat.

TEST PROCEDURE

The shear web and test frame were installed in a 1.2 million pound compression test machine, and restrained laterally as shown in figure 8. The test frame was supported at the bottom on each end and was loaded at the center of the top. The tension bar lateral restraint system did not affect in-plane deformations of the web. The total applied design load for the strength critical web was 550 kips and for the stability critical we was 360 kips.

The shear webs were instrumented with strain gages as shown in figure 9. Each side was instrumented to survey the shear field as well as the beam bending strains. Back to back gages were used up to the limit (98 gages) of the Langley Digital Data Recording System. The gages were primarily oriented at $\pm$ 45° to record shearing strains and horizontally to record beam bending strains. The test frame caps were instrumented as shown in Figure 10.

The moire fringe technique of observing lateral displacements was used to identify the buckling mode shape. Photographs were taken throughout the tests of the changing fringe pattern.

TEST RESULTS

Strength Critical Shear Web

The strength critical shear web was loaded to failure, which occurred at 434 kips. The failed shear web is shown in figures 11(a) and 11(b). Failure is suspected to have initially occurred at a point approximately 13" from the center attachment angle and approximately 7" from the top attachment angle because both compression and tension cracks appear to have run from this region to the panel edges. Moire fringe photographs did not show any discernible lateral displacement at failure. Back to back strain gages showed maximum deviations which were less than approximately $\pm$ 5% from their respective membrane values, indicating that lateral bending was not a significant contributor to failure of the web. Figure 12 shows the $\pm$ 45° strain response from rosettes which surround the central region of the test web. Horizontal and/or vertical strains from these rosettes were sufficiently small that the $\pm$ 45° strains were, in essence, principal values. Thus, the shearing strain magnitude is the sum of the absolute values of principal strain shown in figure 12. Selecting an average value of each strain component at maximum load shows the average value of membrane shearing strain over a large portion of the web to be approximately equal to .0086 in/in just prior to failure.

A force-stiffness plot for the strength critical shear web is shown in figure 13. This web was expected to deform in a linear elastic manner under a shear loading in which case the stiffness (load /strain ratio) is constant and plots as a horizontal line. Therefore, the strain parameter selected to

monitor linear elastic shearing deformation was membrane shearing strain of the faces. Lines of constant, limiting strain are also shown in the figure. Tests to determine the average and B value allowable strains for a pure shear loading only are described in Appendix A. Failure is predicted when the horizontal line (experimental performance) crosses a limiting strength line. The amplitude of the actual load/strain ratio is directly proportional to the inplane structural shear stiffness of the web. Curve I shows the web behavior as assumed during preliminary design. This curve indicates that for the initially assumed stiffness behavior, the design load would be reached before strength failure occurred. However, curve II indicates that the web, in general, did not possess the structural membrane shear stiffness assumed during preliminary design. This curve indicates that, even with the reduced average membrane shear stiffness shown, the web should have reached approximately 488 kips before becoming strength critical. Curve III shows the load shear strain response determined from strain gages 15 and 16. Strain gage 15 indicated the highest compressive strain reading of any gage. It also was the closest gage to the suspected failure point and was approximately aligned along a 45° line (principal compressive strain direction) with the failure point. Therefore, strain gages 15 and 16 give indication that higher strains were present in the area of initial failure. Preliminary finite element analysis also indicates an area of stress concentration near the suspected failure point. However, calculated quantitative results do not yet agree with experimental results. Modeling and material property inaccuracies are currently being investigated. The shear strain behavior described by curve III indicates that the location of SG-'5 and 16 was sufficiently higher stressed

(strained) than the major portion of the web (indicated by curve II) that this location was near the failure load region bounded by the pure shear strength (strain) cutoff lines.

The decreased shear web stiffness, indicated by curve II (and III), as compared to the stiffness indicated by curve I, is believed to be caused by a decreased effective web depth. In curve I, the web depth was taken as 36", which is the full web depth. However, a comparison of the shear stiffness (Gt) of the laminate doubler and attachment angle with the test section shear stiffness, showed the doubler area to have stiffness approximately an order of magnitude larger than the test section. Thus, the shear deformation of the web was apparently concentrated in the area with the smallest stiffness. Using the distance between the inside bolt rows (32.5 inches) as an effective web depth and the experimentally determined shear modulus, the theoretical force stiffness response (see curve IV, figure 13) was generated. Thus, from the agreement of curves IV with curve II, it appears that the decreased overall web membrane shear stiffness (curve II) was, at least, partially due to a reduced effective web depth. Failure at a lower load, as characterized by the deviation of curve III from curve II,may be attributed to localized combined membrane load effects caused by the test method employed.

It is of interest to calculate the membrane shear modulus of the $\pm$ 45° Gr/E material from the large web test for comparison with the material tests given in Appendix A. Figure 14 shows an in-plane shear stress-strain curve from material tests (Appendix A). The structural shear web curves were generated using average values of membrane shear strain and web heights of 36 and 32.5 inches. Using the full web height of 36 inches results in a

shear modulus of 5.31 x 10^6psi. Using the effective height of 32.5 inches results in a shear modulus of 5.88 x 10^6psi, which agrees well with the material test value.

Load deflection curves are shown in figure 15 for the vertical displacement at the bottom of the beam center. The measured deflection was approximately 30% larger than that predicted by an initial NASTRAN analysis, giving additional indication of the web's reduced stiffness. Figure 16 shows the measured cap strains at the center of the test frame. As shown in figure 10, the caps were formed from three-1/2" thick aluminum plates bolted together. Strain gage 93 was attached to the edge of the middle plate in the top cap and strain gage 83 was attached to the surface of the outside plate in the bottom cap. Both gages are shown in figure 16 to exhibit nonlinear behavior and show a decreasing strain rate with load. This indicates ineffectiveness of the outer plates in carrying cap-loads, requiring the inner plates to be strained higher to react the external forces. Also included in figure 16, are the cap strains predicted by strength of materials and by an initial NASTRAN analysis. The strength of materials results assume that only the caps react the external forces. The NASTRAN results indicate that the caps only carry approximately 80% of the beam bending load predicted by strength of materials. Comparison of NASTRAN and experimental results indicate that the frame caps had less extensional stiffness than originally assumed partially due to ineffectiveness of the outer cap plates.

Figure 17 shows the beam bending strain response along vertical lines at various stations along the test web. Station A1 (see figure 9 for station location) curves show the horizontal strain response at the web attachment to

the beam center-post. Strain gages 7 and 55 were at the top of the web and theoretically should have indicated compression instead of tension as is shown. Thus, along the beam centerpost the web did not carry any beam bending. This effect is still evident at station A2, which is at an interior location to station A1, where strain gage 61 shows tension. Strain gages 17 and 61, at low loads, originally showed slightly higher tension values but either remained constant (61) or went into compression (17) at higher loadings, indicating that some internal load redistribution was occurring as the external load was increased. Strain gage response at stations A3 and A4 indicate that the beam neutral axis was very near to the bottom cap area at these locations. The ineffectiveness of the outer cap plates and the internal load redistribution distort test web performance and make meaningful comparison with analysis extremely tenuous.

Stability Critical Shear Web

The stability critical shear web was loaded to failure, which occurred at 248 kips. The failed shear web is shown in figure 18(a) and (b). Considering figure 18(b), it appears that failure initially occurred in the compressive stress direction in the upper left hand quadrant of the panel. Tension cracks are shown to run from a compressive failure strip toward the panel edges. These tension cracks apparently were generated as a result of the compressive failure. A moire fringe photograph is shown in figure 19. This photograph was taken at 240 kips and clearly shows the formation of one large skewed buckle. The effect of the initial panel curvature may be seen in figure 20. Divergence of back-to-back strain gage responses, which were located across the center of the panel show that lateral bending occurred

from the onset of loading with strain gage reversal occurring at approximately 220 kps. The strain gage responses shown in figure 20 indicate that the bending deformations were not localized but rather, involved the entire web. The overall, average membrane shear strain of the web at failure was also determined from the strain gage responses shown in figure 20. Using the average membrane values of compressive and tensile strains, the average membrane shear strain was found to be .006 in/in at failure.

A force-stiffness plot based on membrane shear strain is shown in figure 21 for the stability critical web. The strength allowable curves shown in figure 21 are only applicable to material loaded in pure membrane shear, and do not directly apply to a test which includes transverse bending (involving possible core failure modes) and/or combined membrane loads, all of which occurred in this test. The preliminary design (curve I) estimate of web membrane shear stiffness indicates a sizable strength margin at the design buckling load of 360 kips. Curve II indicates that even with the reduced membrane stiffness, and linear behavior, the web should have reached 360 kips prior to becoming strength critical. The curve III results were computed from strain gages 11 and 12 which were the highest reading gages on the web. These results indicate that an area of increased strain occurred in the top quadrant of the web near the unloaded corner due primarily to transverse bending of the web. This is also the area where material failure is thought to have initially occurred. From the magnitude of the recorded strains, it appears that the web failed in the compressive filamentary direction. While the quantitative effects of transverse bending (or buckling) and/or combined load on material strength is undetermined, the qualitative effect indicates a sizable reduction from the membrane strength allowables.

The stability critical shear web exhibited reduced membrane shear stiffness prior to failure, in the same manner as the strength critical web. Previous comments and observations about material shear modulus and effective web depth are also applicable here.

Figure 22 shows a comparison of the theoretical and experimental midpoint deflections of the test beam. The measured deflection was approximately 35% greater than was predicted by an initial NASTRAN model. This deviation is approximately the same as occurred with the strength critical web. Figure 22 is a comparison of the measured and theoretical cap strains. During this test, strain gage 93 was installed on the edge of the outside plate of the top cap, and indicated that the outside cap plates were ineffective in carrying the compressive load. Response from strain gage 83 indicates closer agreement with predicted performance than does strain gage 93. However, this was apparently the result of slippage of the outside cap plate as indicated by a shift in the strain gage response. Beam bending strains along the centerpost showed the same tensile behavior as the strength critical web (figure 17). Therefore, it appears that the frame behavior was similar for both shear webs tested.

Weight-Strength Performance

A summary of the strength critical and stability critical test web performance is given in Table 4. The strength critical web attained approximately 79% (6028 lb/in) of the preliminary design goal (7638 lb/in.

and developed facing shear stresses in excess of 50,000 psi without exhibiting instability or any appreciable degree of nonlinear behavior.

The stability critical web attained approximately 69% (3444 lb/in) of the preliminary design goal (5000 lb/in) and developed facing shear stresses in excess of 40,000 psi prior to failure. However, this web did exhibit transverse bending behavior from the onset of loading due to initial panel curvature and a thinner sandwich core than the strength critical web.

The weight-strength characteristics of various shear web constructions are shown in figure 24, where test section weight per unit area per unit depth (W/Ab) is plotted versus the shear load per unit depth (N_{xy}/b). The shaded area of figure 24 bounds the region over which aluminum data (summarized in reference 4) was generated by the NACA. The solid curves are theoretical predictions (reference 5) which show the limiting behavior for various structural concepts. The experimental stability critical performance of the Ti-clad B/E web (No. 3) of reference 1 is also shown in the figure. The dashed line is a theoretical prediction of strength critical Gr/E sandwich behavior for the web tested. The stability critical web should be compared to the curve segment indicated and not to the strength critical curve. Both the strength critical and stability critical web experimental results were plotted using full web depth of 36" instead of the "effective" depth of 32.5". The strength critical web (N_{xy}/b = 167 lb/in/in) is shown to weigh approximately 1/3 as much as the most efficient aluminum structure at that load index and approximately 46% as much as the Ti clad B/E web. Although greatly influenced by initial curvature, the stability critical shear web (N_{xy}/b = 96 lb/in/in) weighed approximately 1/2 as much as an aluminum structure which would carry the same load.

CONCLUDING REMARKS

Results of an experimental evaluation of two large, heavily-loaded graphite-epoxy shear webs have been presented. The shear webs were of sandwich construction with one specimen designed to exhibit material strength failure of the facings at 7638 lb/in. The second web was designed to exhibit general instability failure at 5000 lb/in. Test results show that the strength critical web failed at approximately 79% of its anticipated load due partially to decreased structural stiffness (i.e. effective web depth and ineffective cap problem) and to combined-load effects caused by the test method employed. Experimental results also indicate that internal load redistribution occurred which was caused primarily by ineffectiveness of the frame cap plates in reacting the external load.

Test results for the stability critical shear web show that failure occurred at 69% of its anticipated buckling load. Differences between the calculated preliminary design value and experimental results were due primarily to sensitivity of this web (thinner core) to initial out-of-plane displacements induced during manufacturing.

In spite of the lower-than-anticipated failures which occurred, the graphite epoxy sandwich shear webs have outstanding weight strength characteristics. The webs achieved shear stresses of 40 to 50 ksi, and were found to be 50% to 67% lighter than the most efficient aluminum structures known.

REFERENCES

1. Laakso, J. H.; and Straayer, J. W.: Evaluation of a Metal Shear Web Selectively Reinforced with Filamentary Composites for Space Shuttle Application. NASA CR-2409, August 1974.

2. Housner, J. M.; and Stein, M.: Numerical Analysis and Parametric Studies of the Buckling of Composite-Orthotropic Compression and Shear Panels. NASA TN D-7996, 1975.

3. Jones, R. E.; and Greene, B. E.: The Force/Stiffness Technique for Nondestructive Buckling Testing. AIAA Paper No. 74-351 presented at the AIAA/ASME/SAE 15th Structures, Structural Dynamics and Materials Conference, Las Vegas, Nevada, April 17-19, 1974.

4. Shanley, F. R.: Weight-Strength Analysis of Aircraft Structures. Second Edition, Dover Publication, Inc., 1960.

5. Gerard, G.; and Becker, H.: Handbook of Structural Stability, Part VII-Strength of Thin-Wing Construction. NASA TN D-162, September 1959.

Table 1.- Preliminary Design Lamina Elastic Properties

	Tension	Compression
E_1	23.5×10^6 psi	19.6×10^6 psi
E_2	2.39×10^6 psi	2.10×10^6 psi
G_{12}	0.76×10^6 psi	0.76×10^6 psi
ν_{12}	0.318	0.318

Table 2.- Theoretical Laminate Elastic Properties

	$\pm$ 45° Laminate
E_x	2.72×10^6 psi
E_y	2.72×10^6 psi
G_{xy}	5.65×10^6 psi
ν_{xy}	0.78

Table 3.- Experimental Laminate Properties

	$\pm$ 45° Laminate	
	Average	"B"
$\tau_{xy_{ult}}$	65,560 psi	58,200 psi
$\gamma_{xy_{ult}}$	.01095 in/in	.00972 in/in
G_{xy}	5.99×10^6 psi	
E_x, E_y	2.8×10^6 psi	

Table 4.- Summary of Results

	Ultimate Load		Experiment / Theory	Total Web Weight
	Theory	Experiment		
Strength Critical Web	7638 lb/in	6028 lb/in	.79	34.1 lb
Stability Critical Web*	5000 lb/in**	3444 lb/in	.69	24.75 lb

* Exhibited nonlinear behavior due to curvature

** Linear-Elastic Calculation

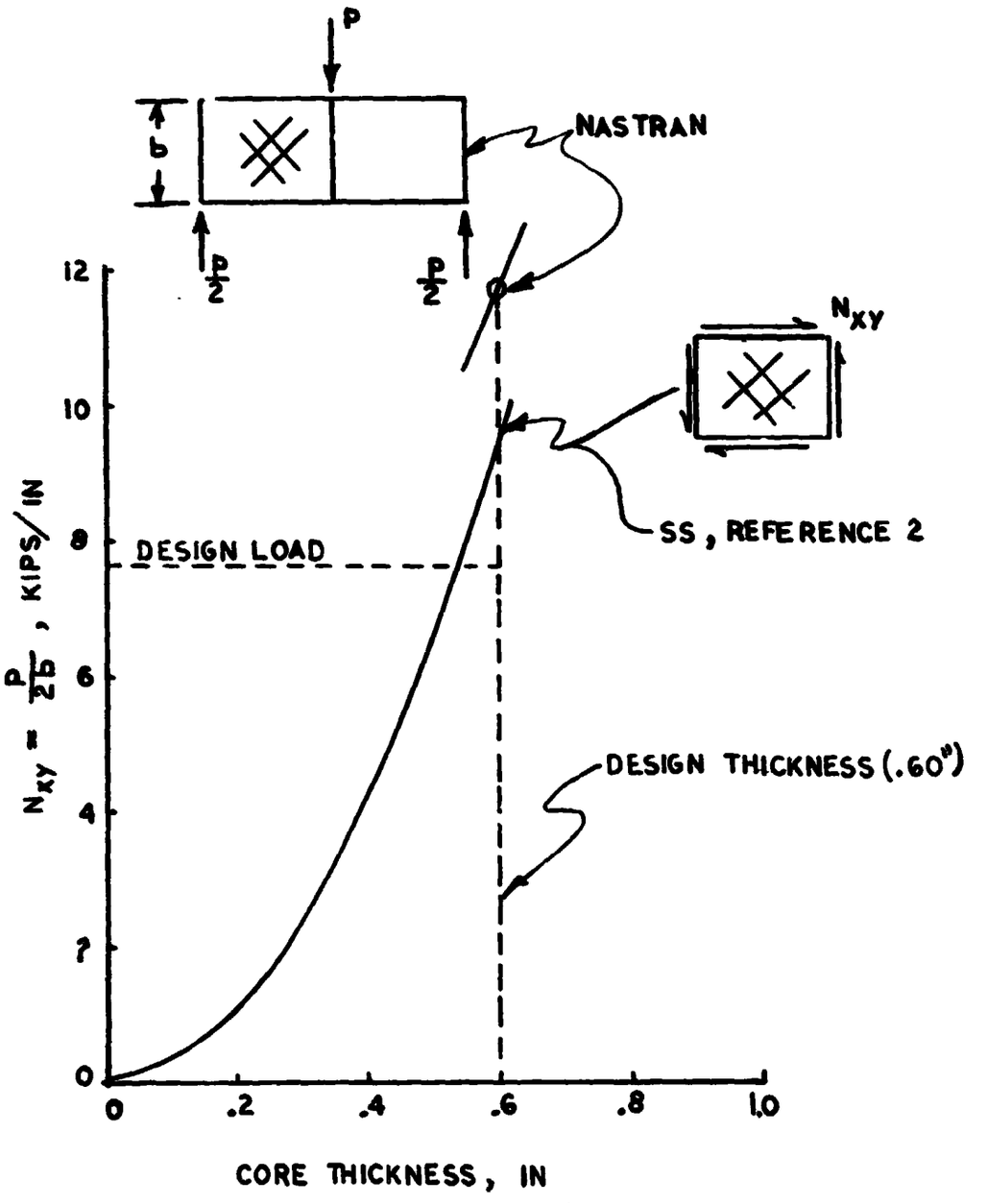

Figure 1.- Theoretical shear buckling load for 36" x 47" webs with .066" Gr/E faces vs core thickness.

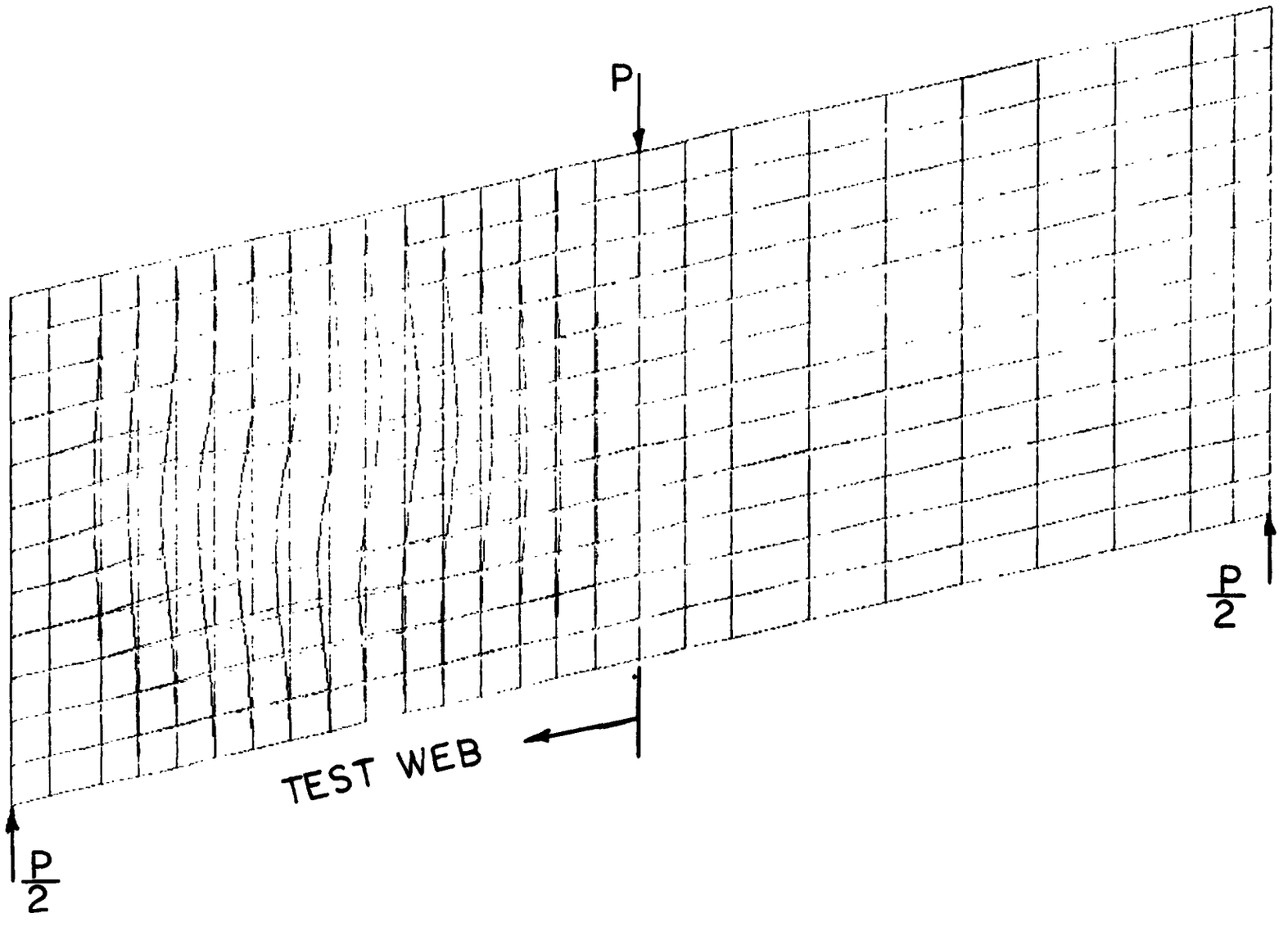

Figure 2.- NASTRAN buckling mode for strength critical shear web (P_{crit} = 846 kips).

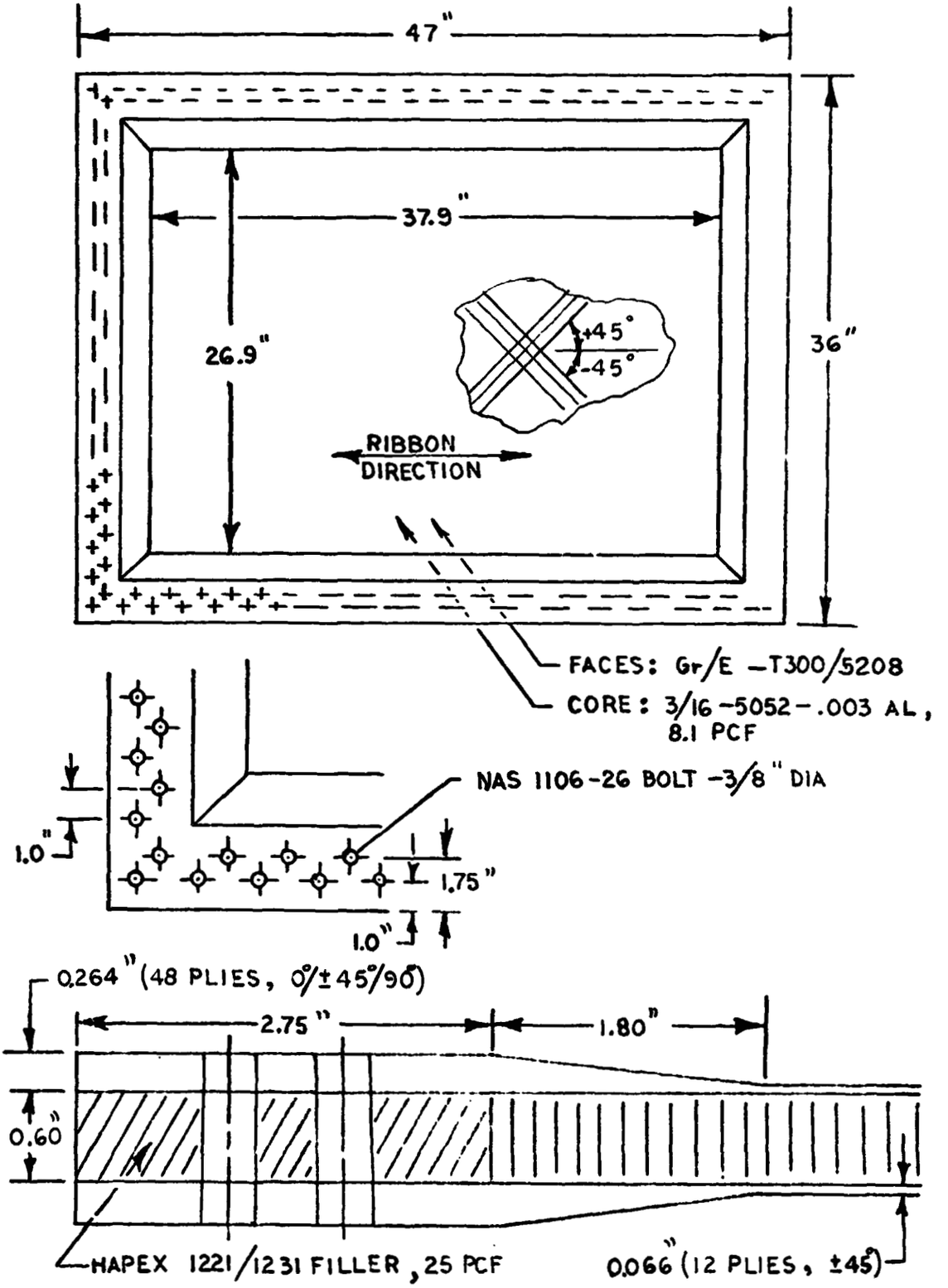

Figure 3.- Design details for strength critical shear web.

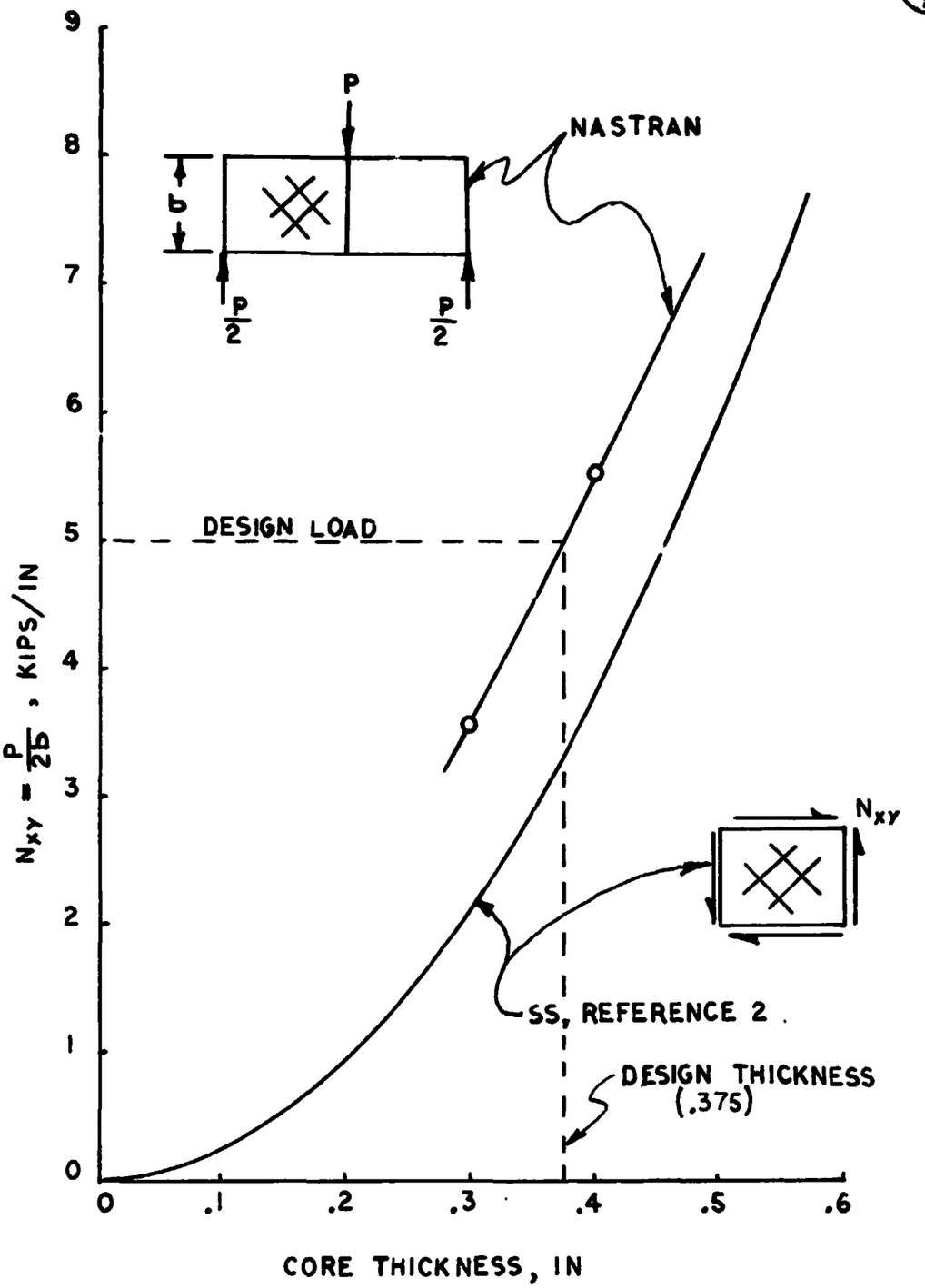

Figure 4.- Theoretical shear buckling load for a 36" x 47" sandwich web with .055" Gr/E faces vs core thickness.

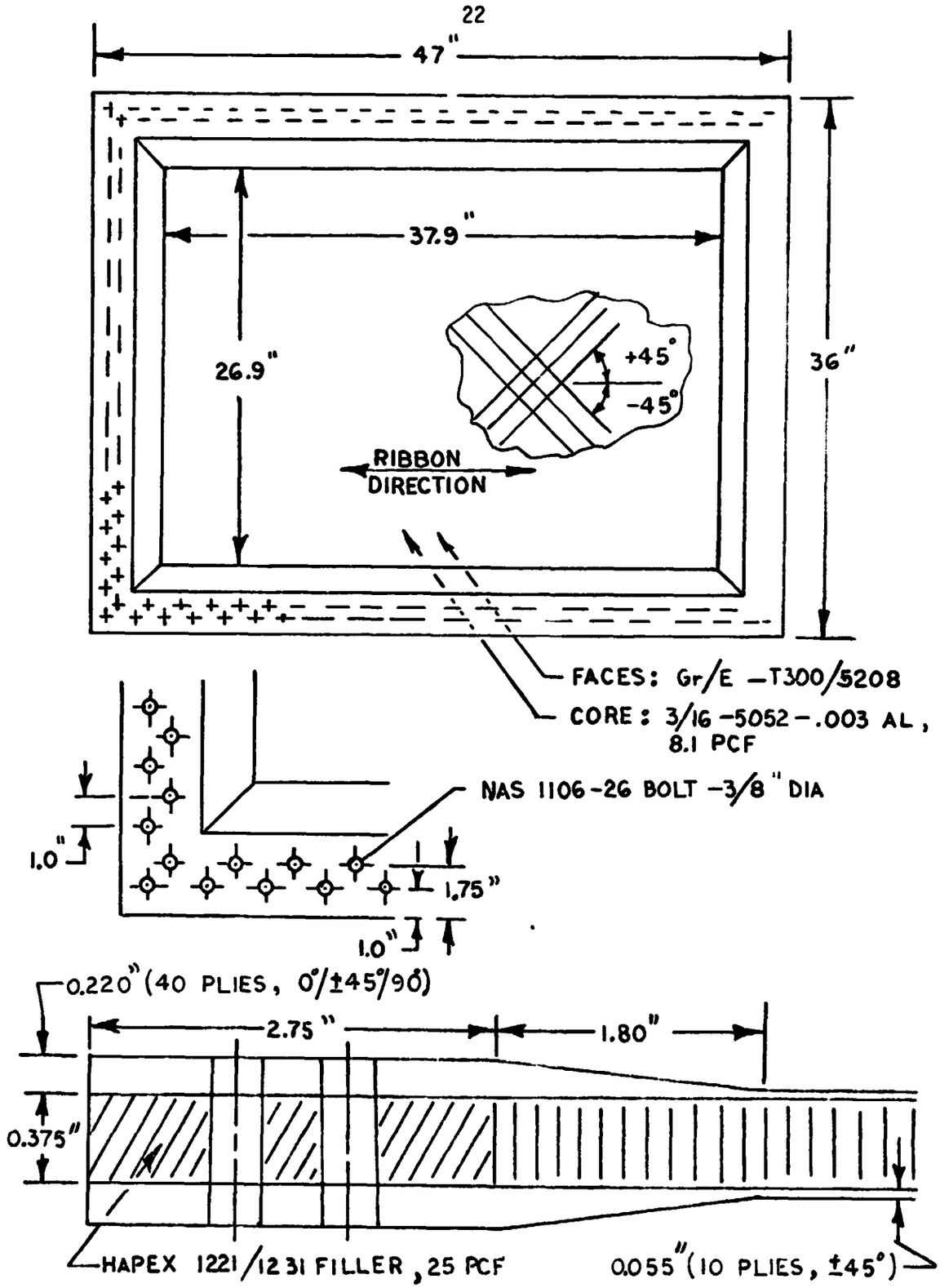

Figure 5.- Design details for stability critical shear web.

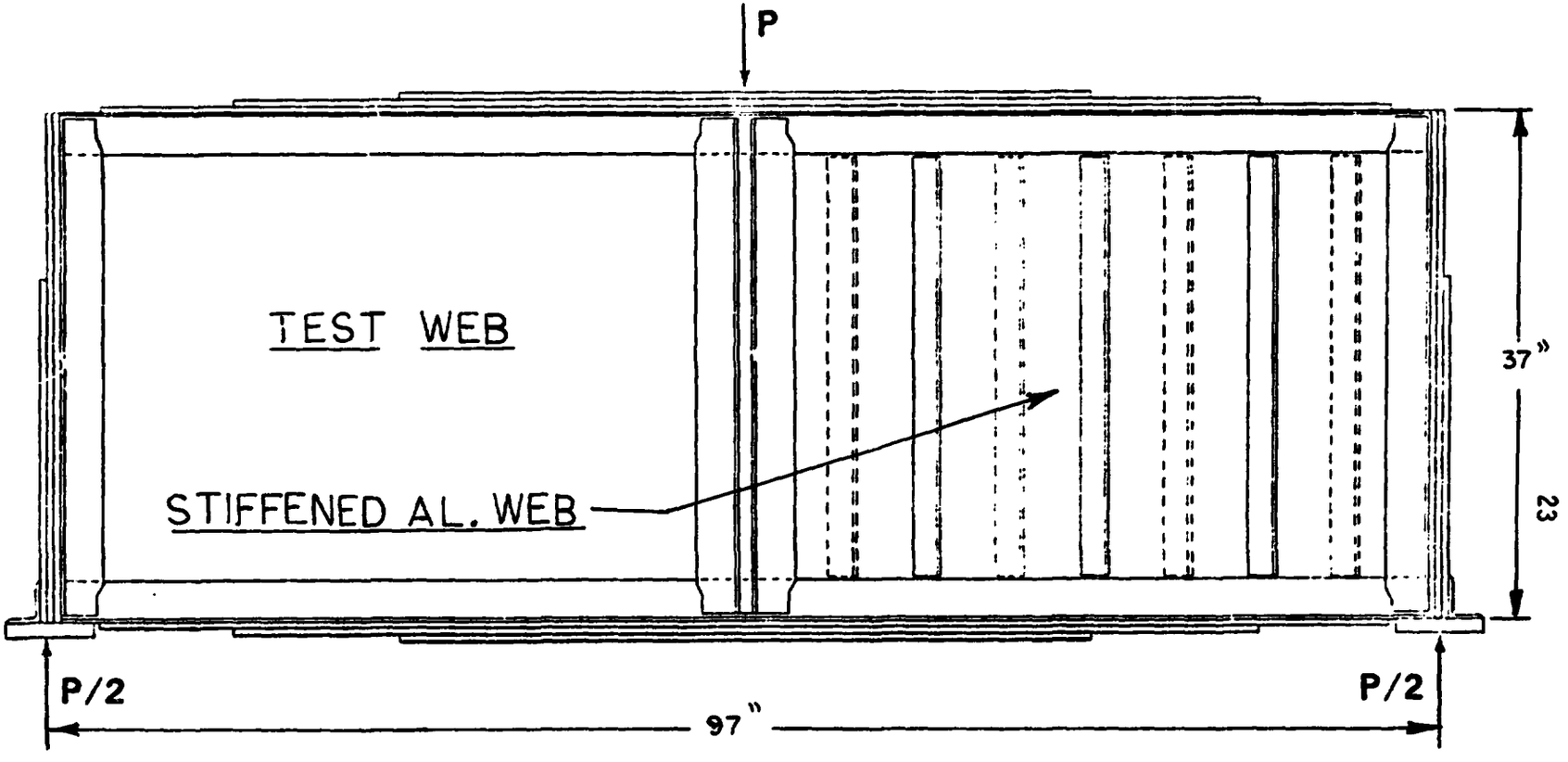

Figure 6.- Shear web test frame.

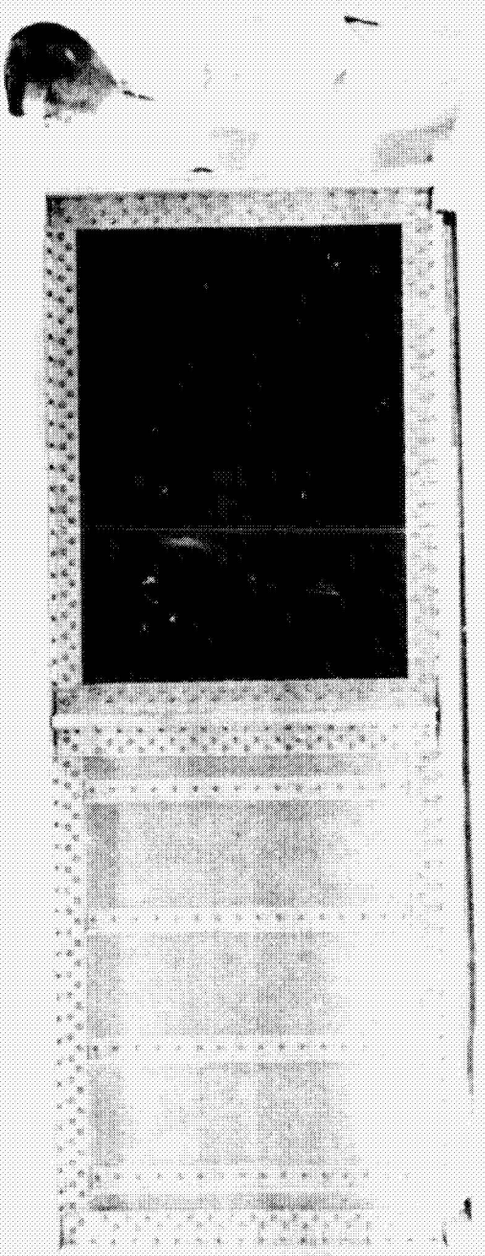

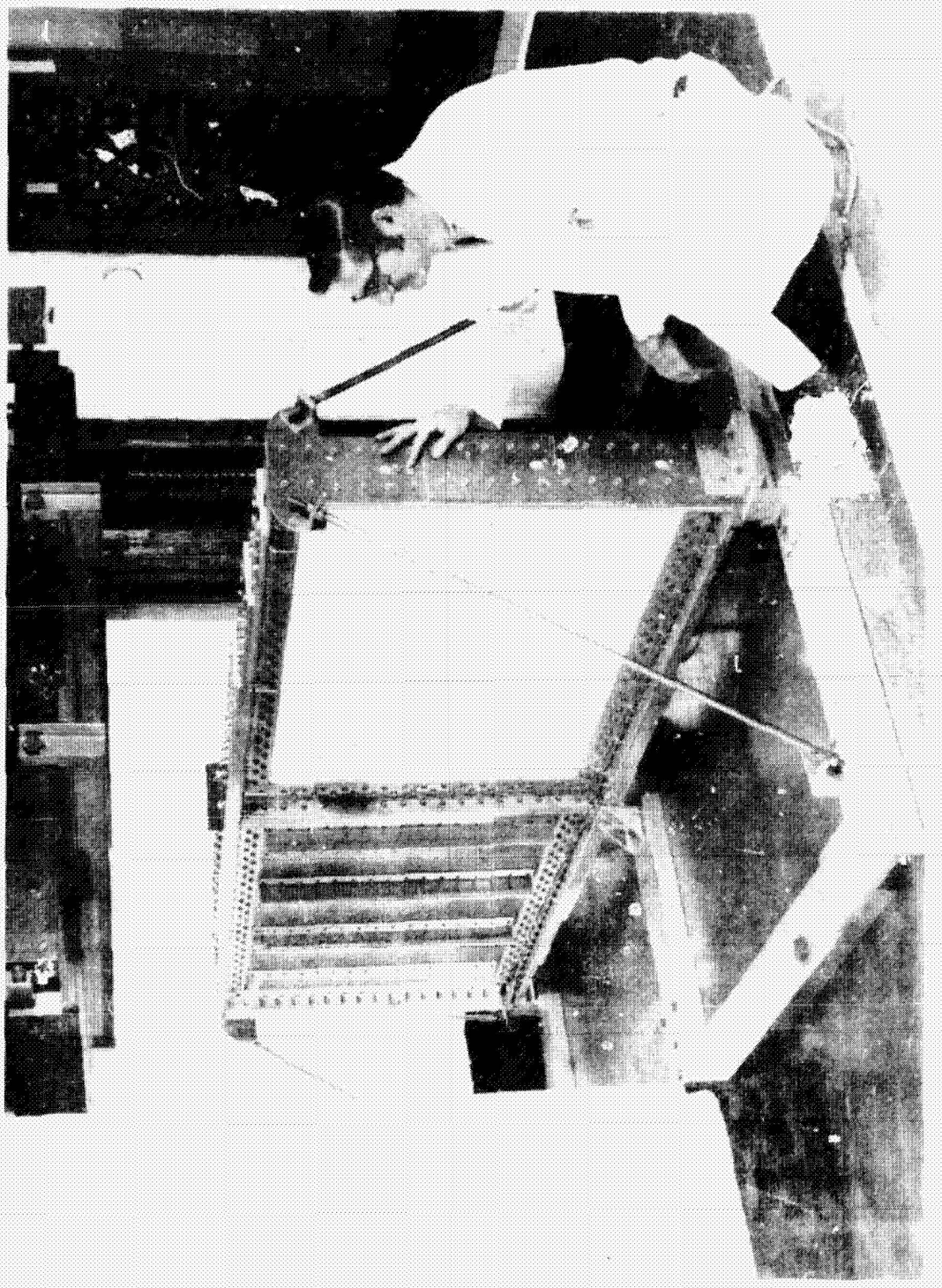

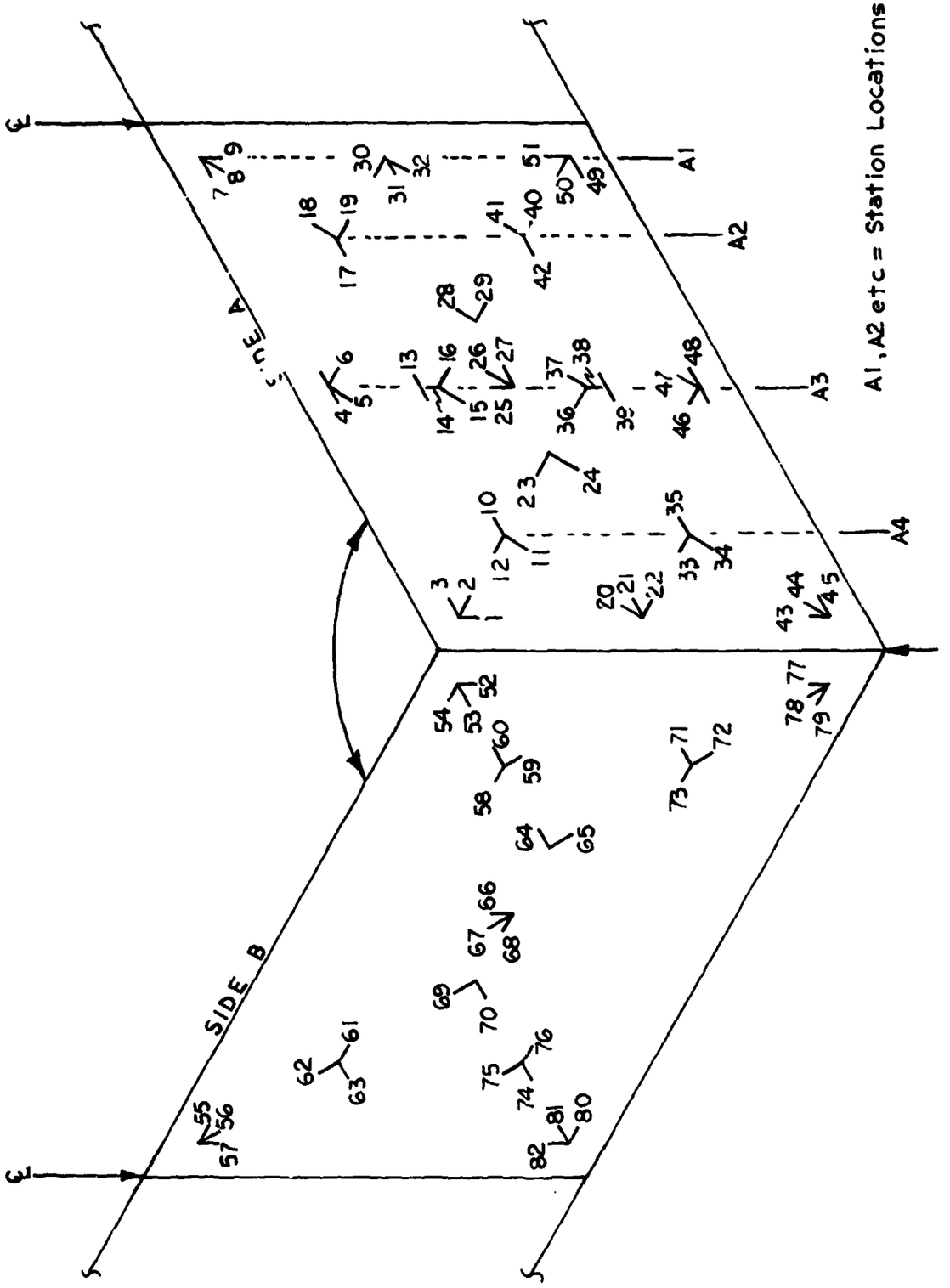

Figure 9.- Sandwich shear web strain-gage layout.

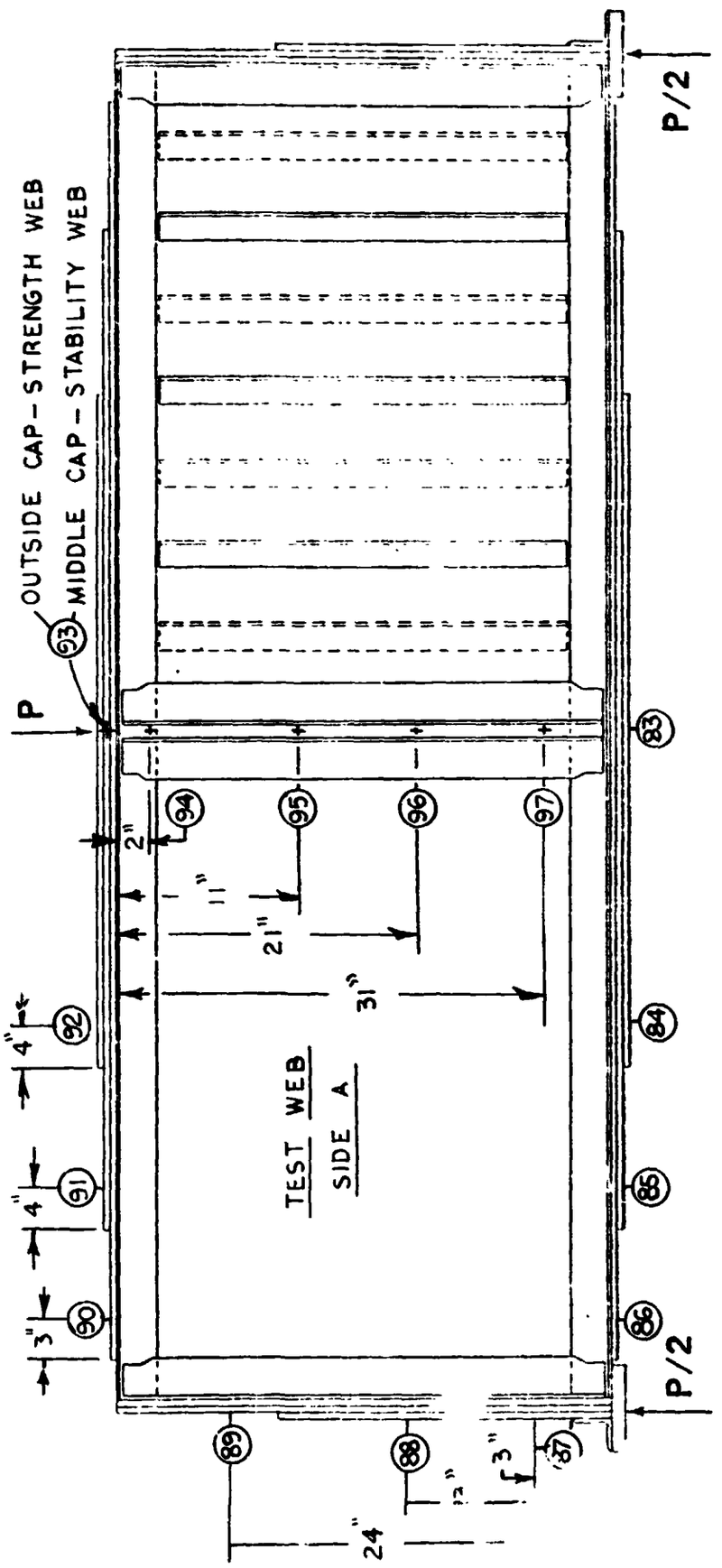

Figure 10.- Shear web test frame instrumentation layout.

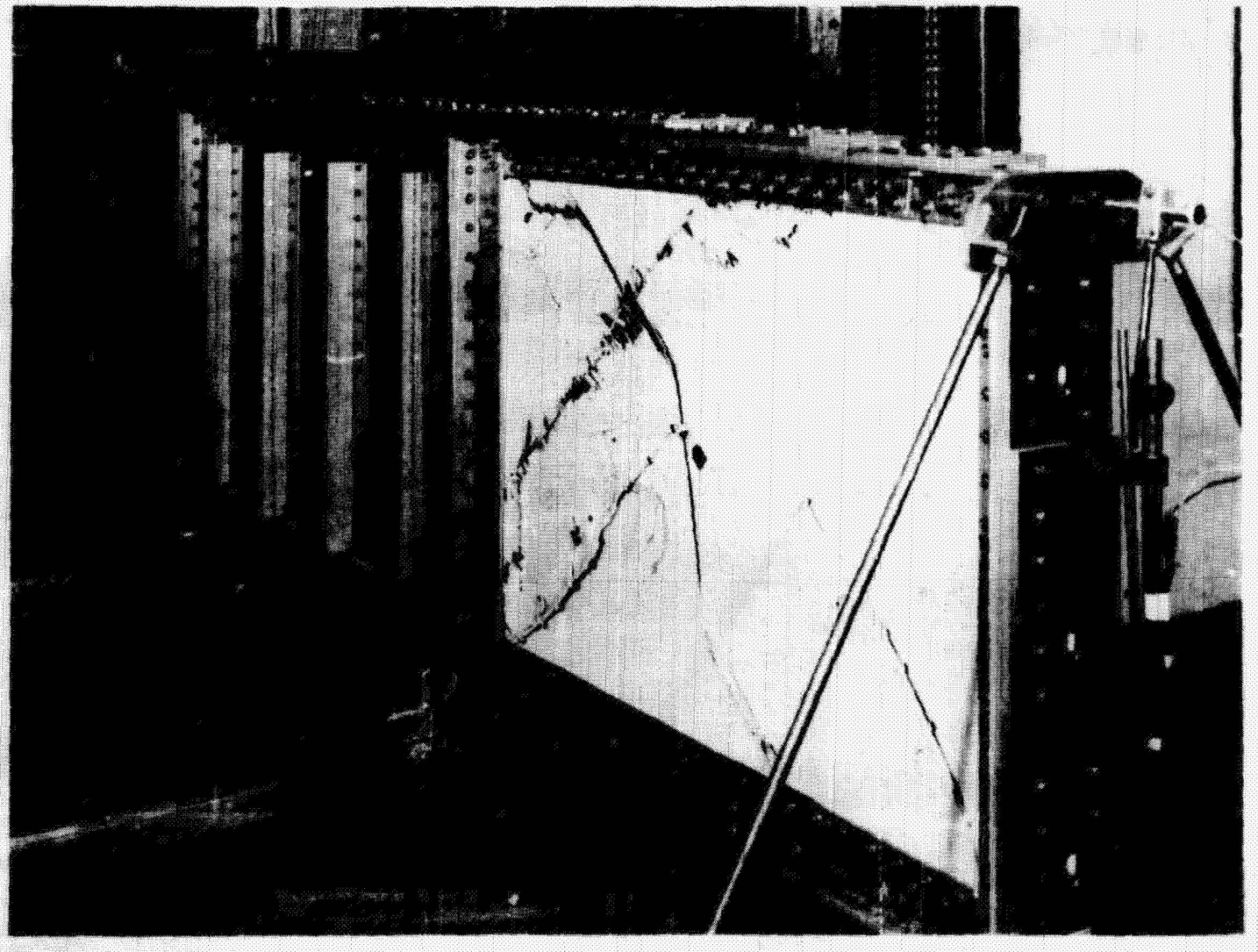

Figure 11(a).- Strength critical shear web after test (Side B).

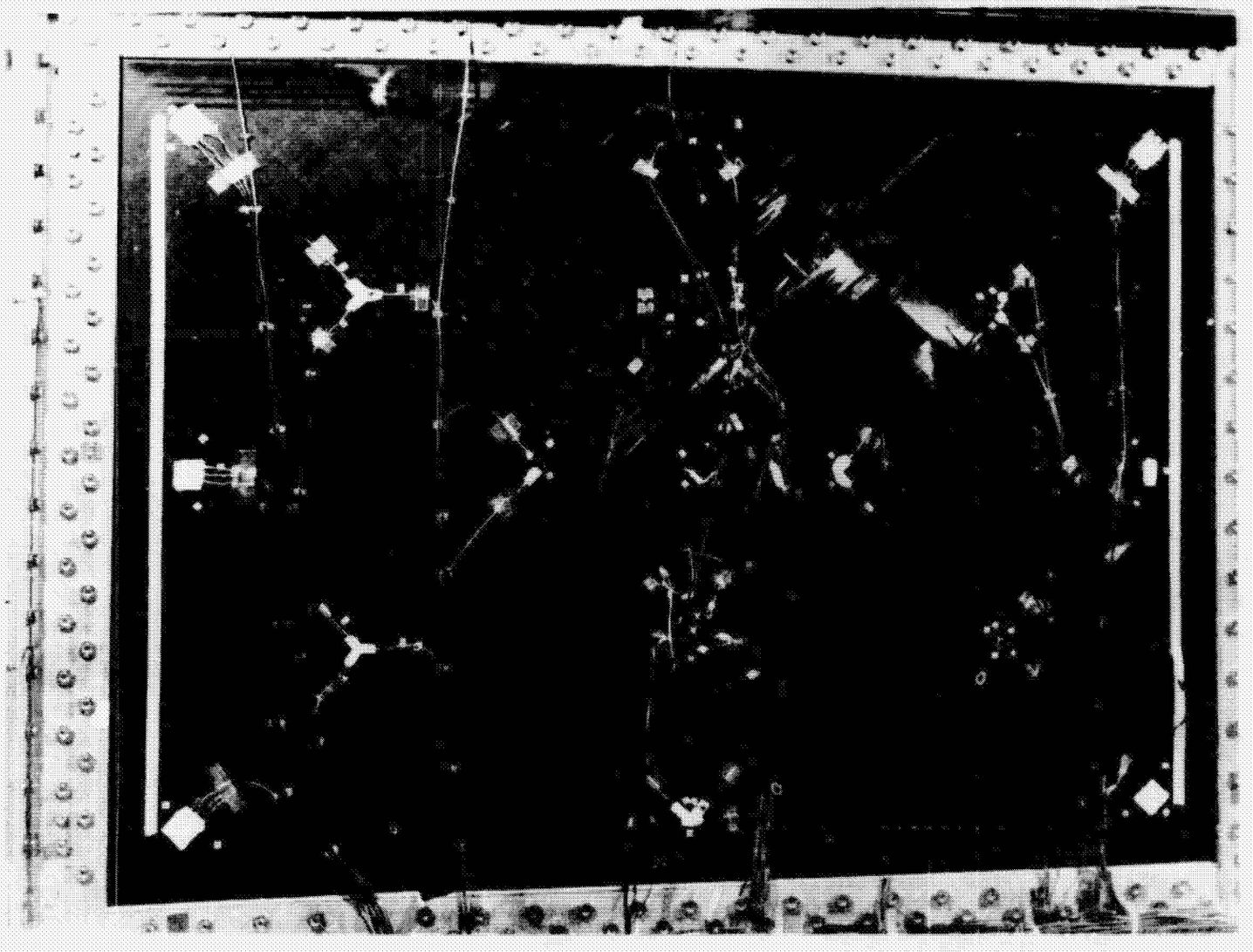

Figure 11(b).- Strength critical shear web after test (Side A).

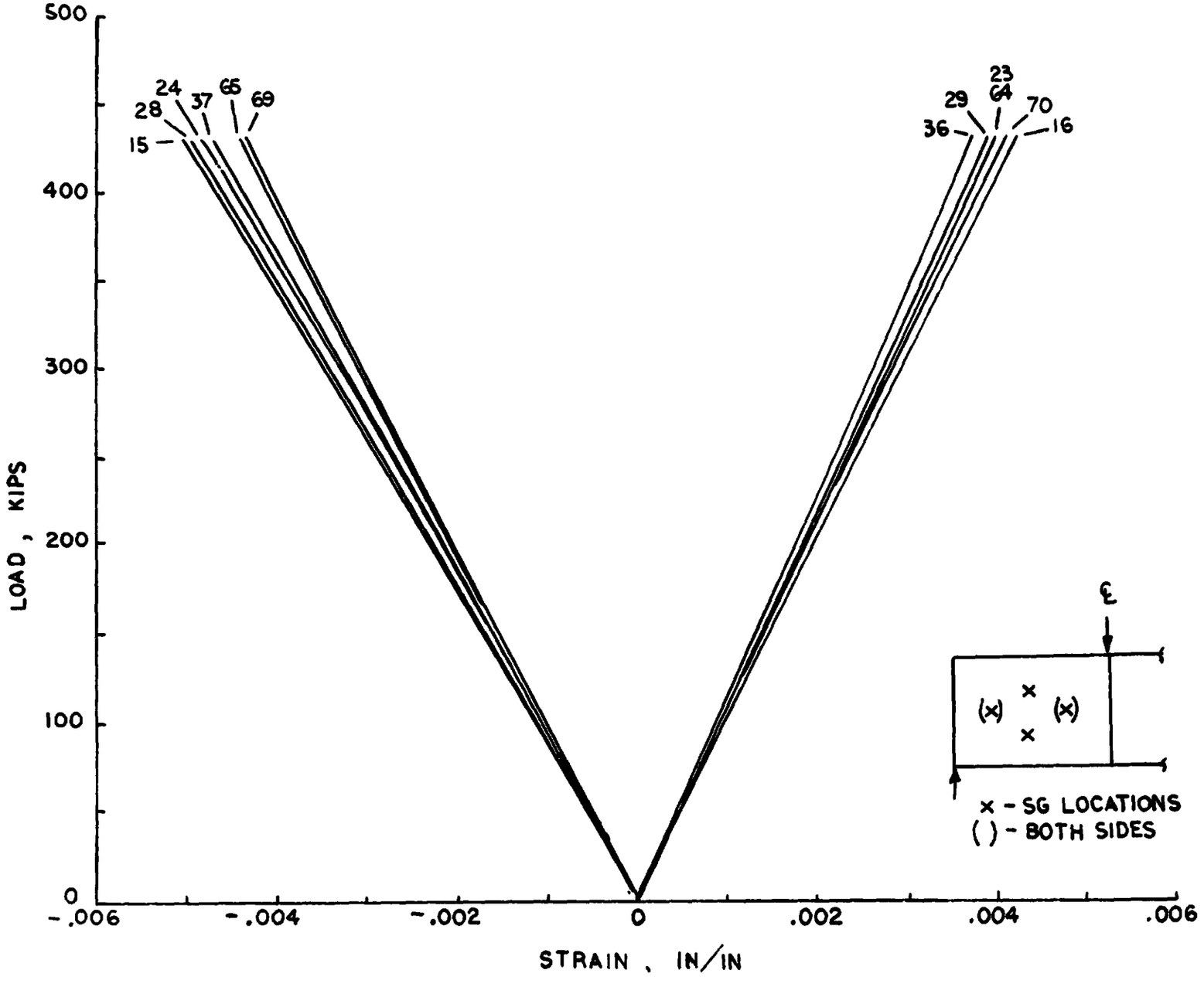

Figure 12.- Strength critical shear web: ± 45° strains vs load.

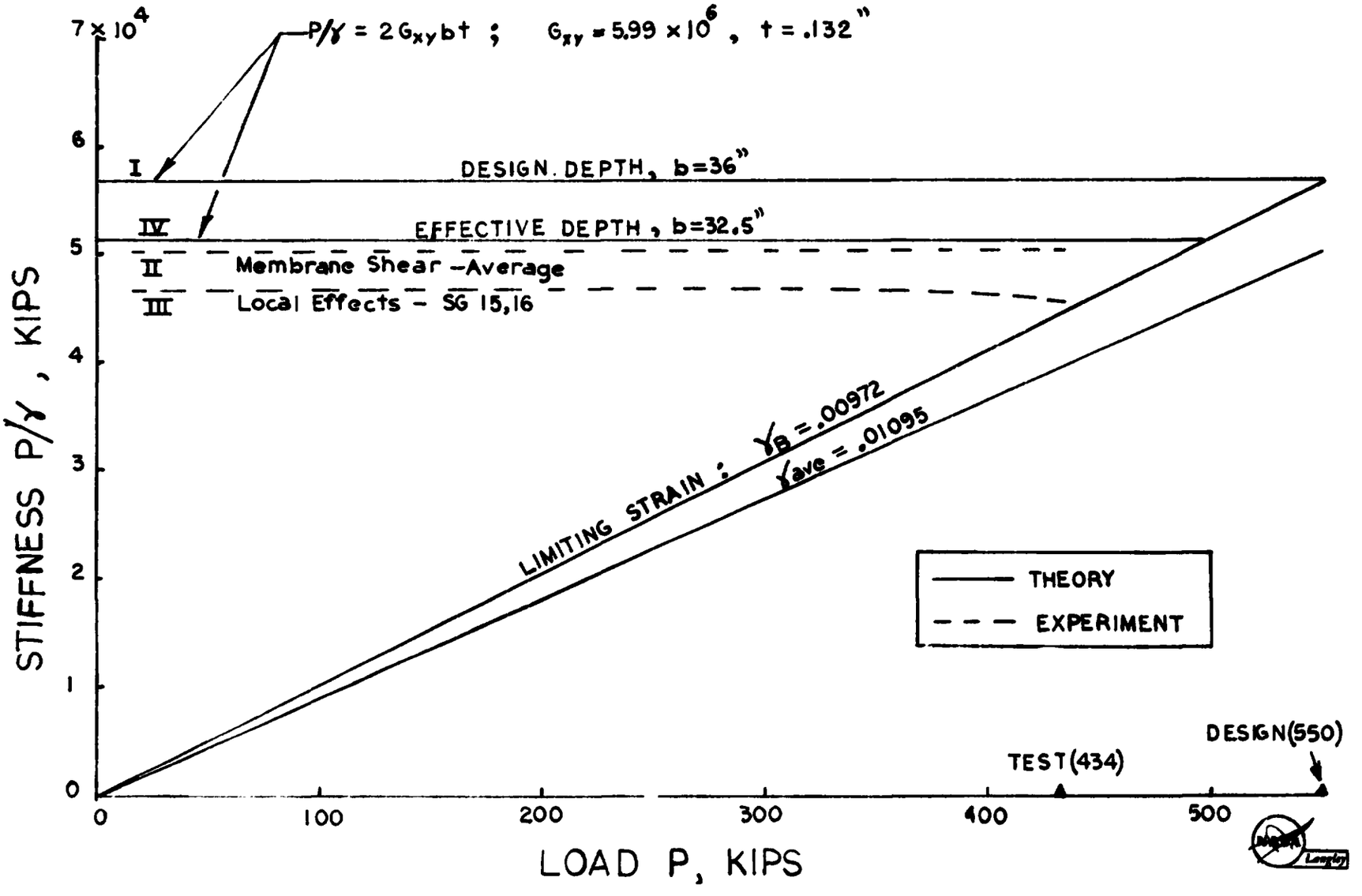

Figure 13.- Force stiffness plot for strength critical shear web.

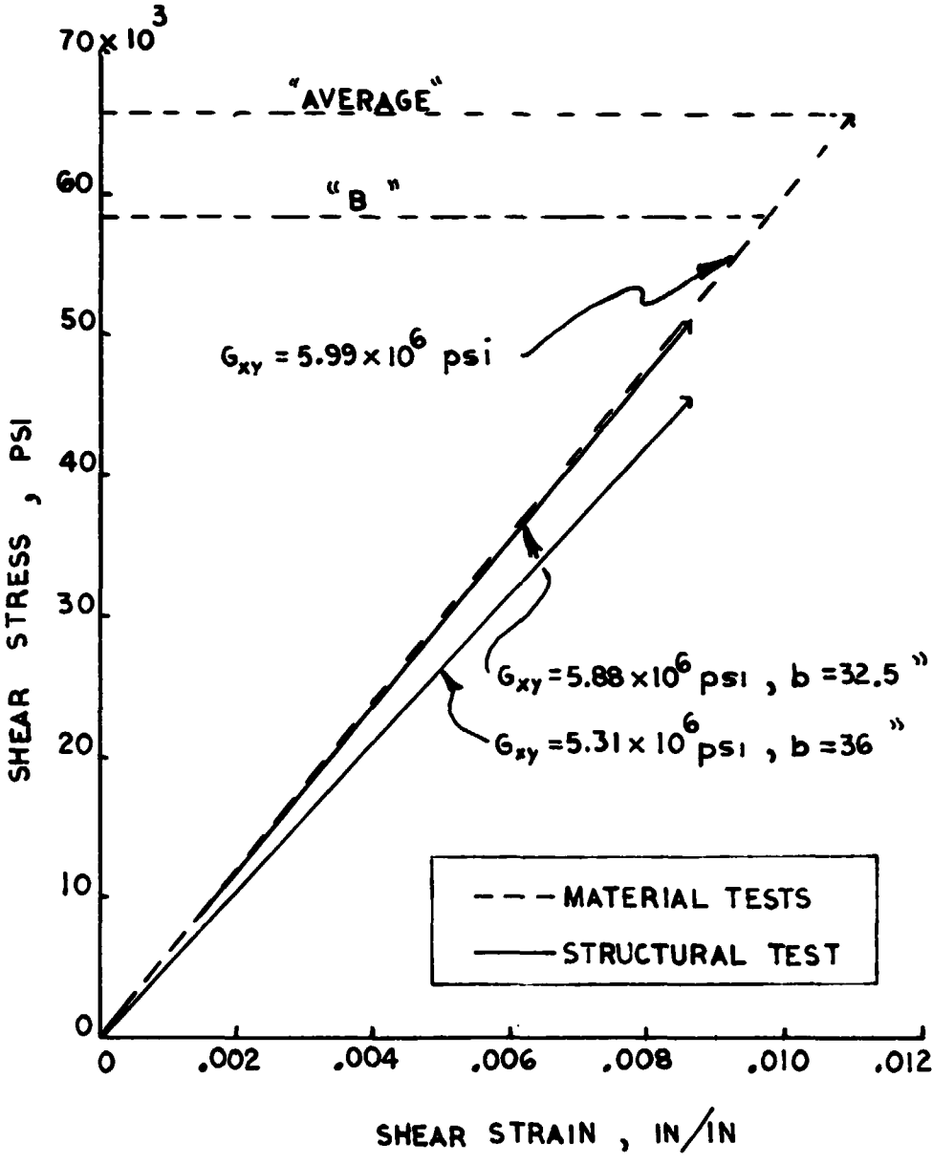

Figure 14.- Inplane shear stress-strain response of ± 45° Gr/E (T300/5208).

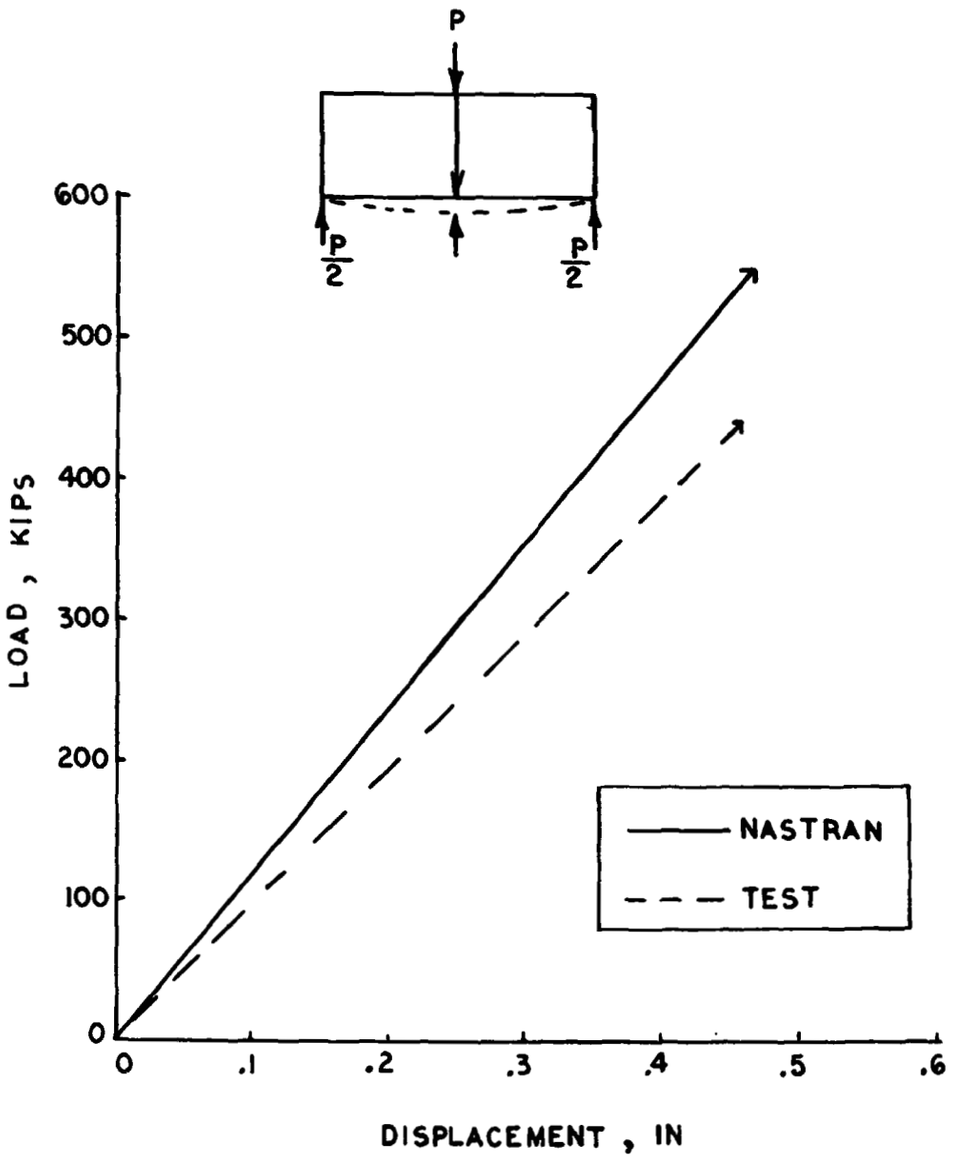

Figure 15.- Vertical displacements at centerline of strength critical web.

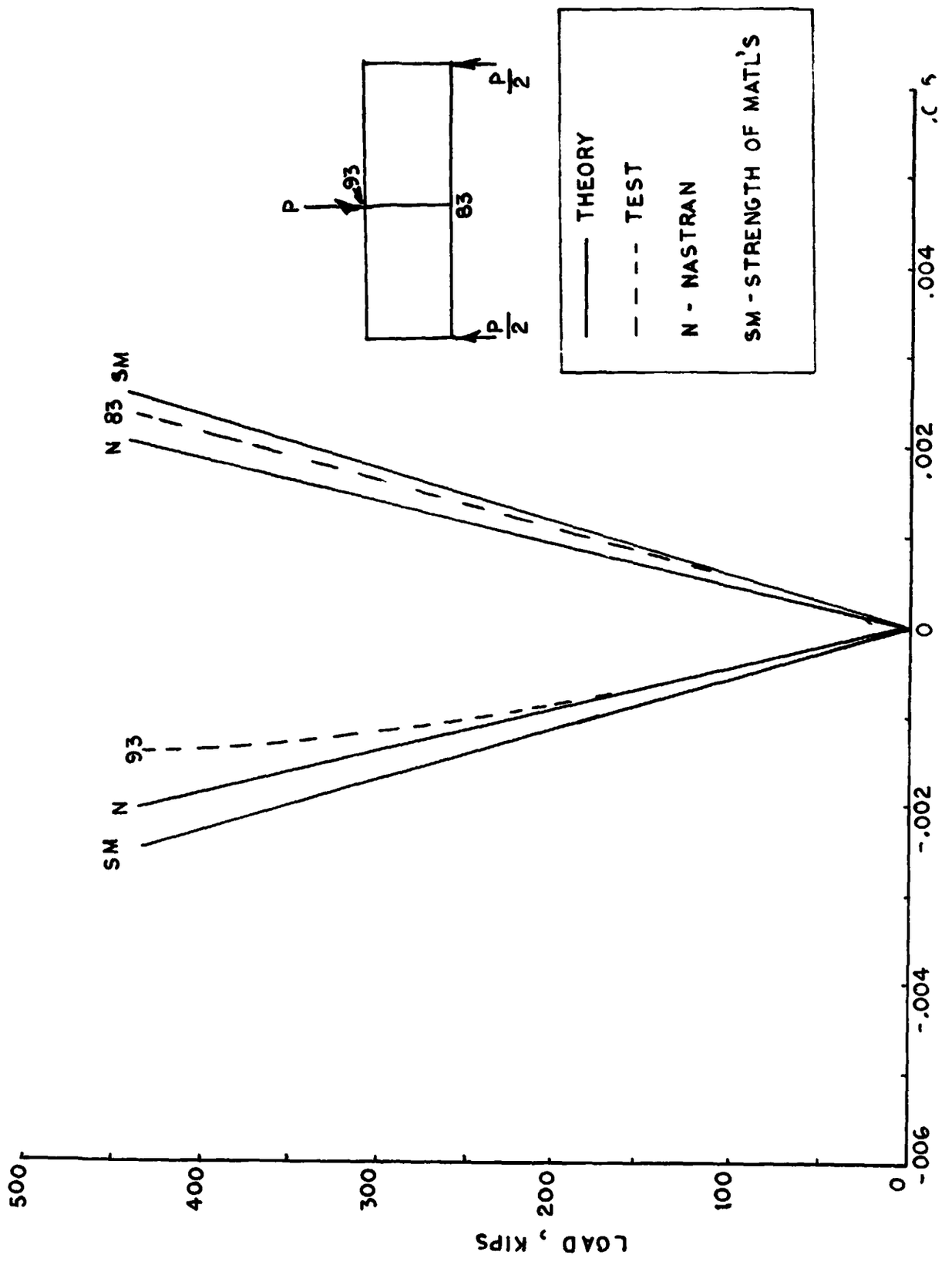

Figure 16.- Cap strains at center of test frame (strength critical web).

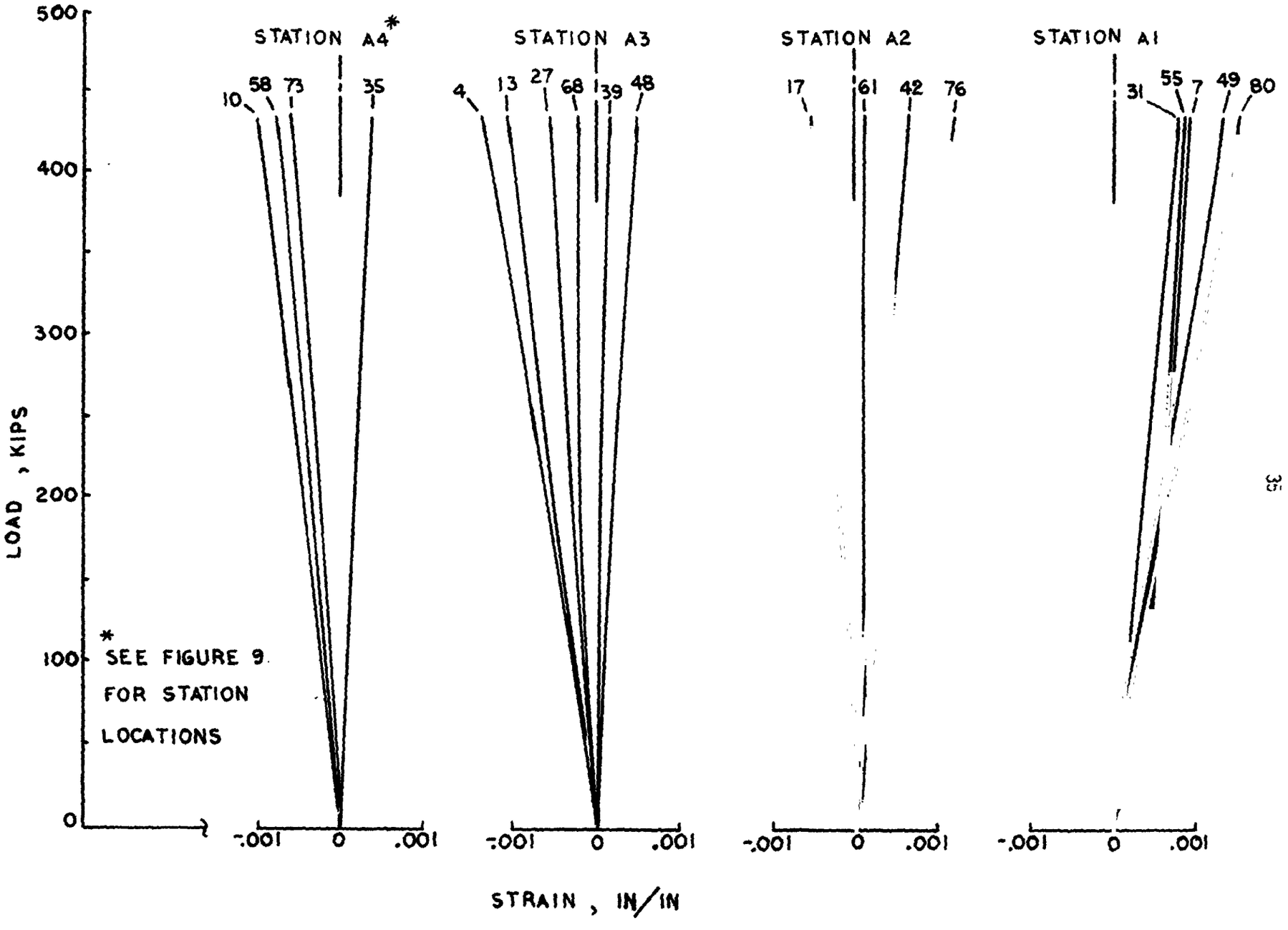

17 - Beam bending (horizontal) strain distribution through web depth

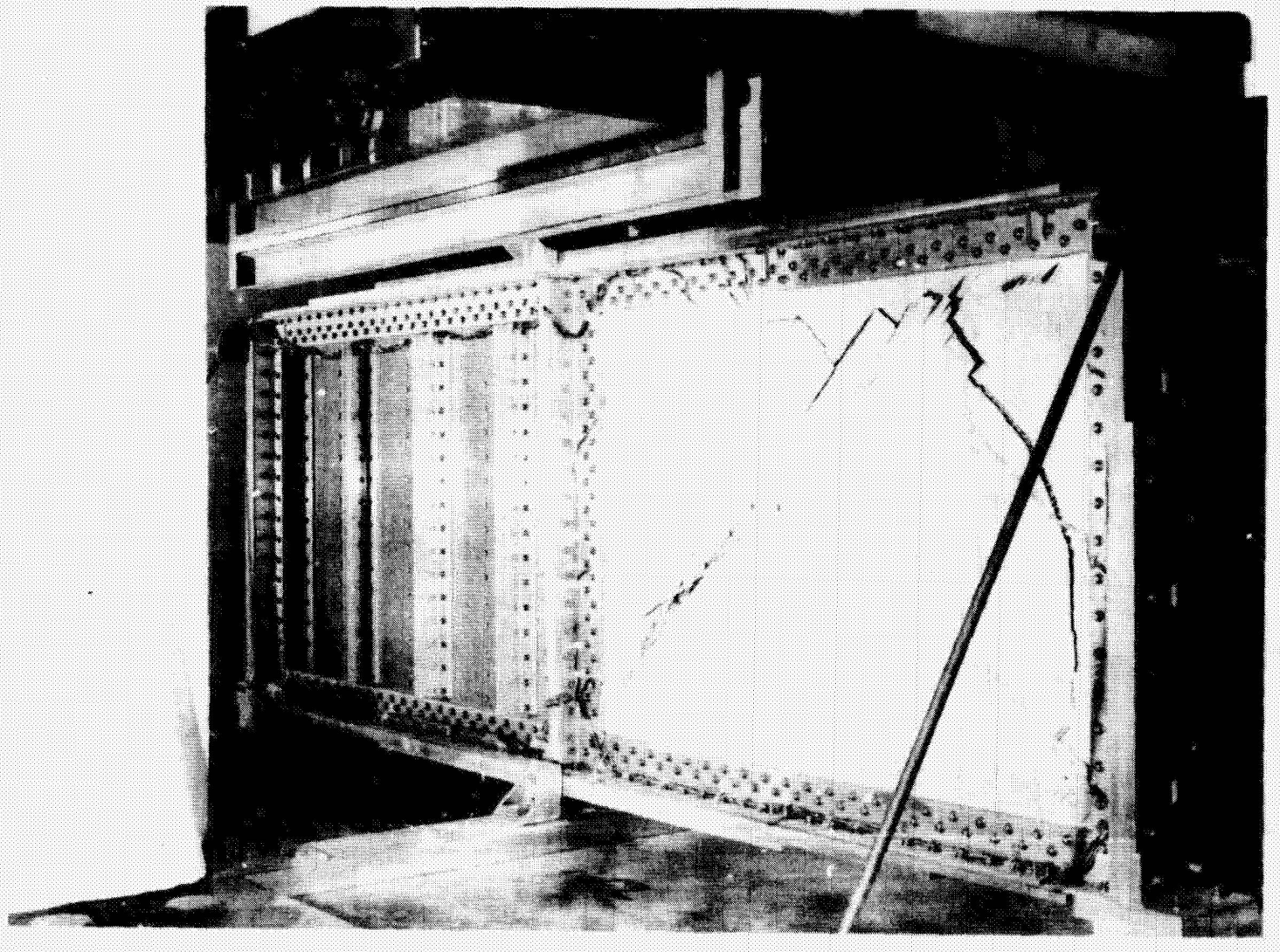

Figure 18(a).- Stability critical shear web after test (Side B).

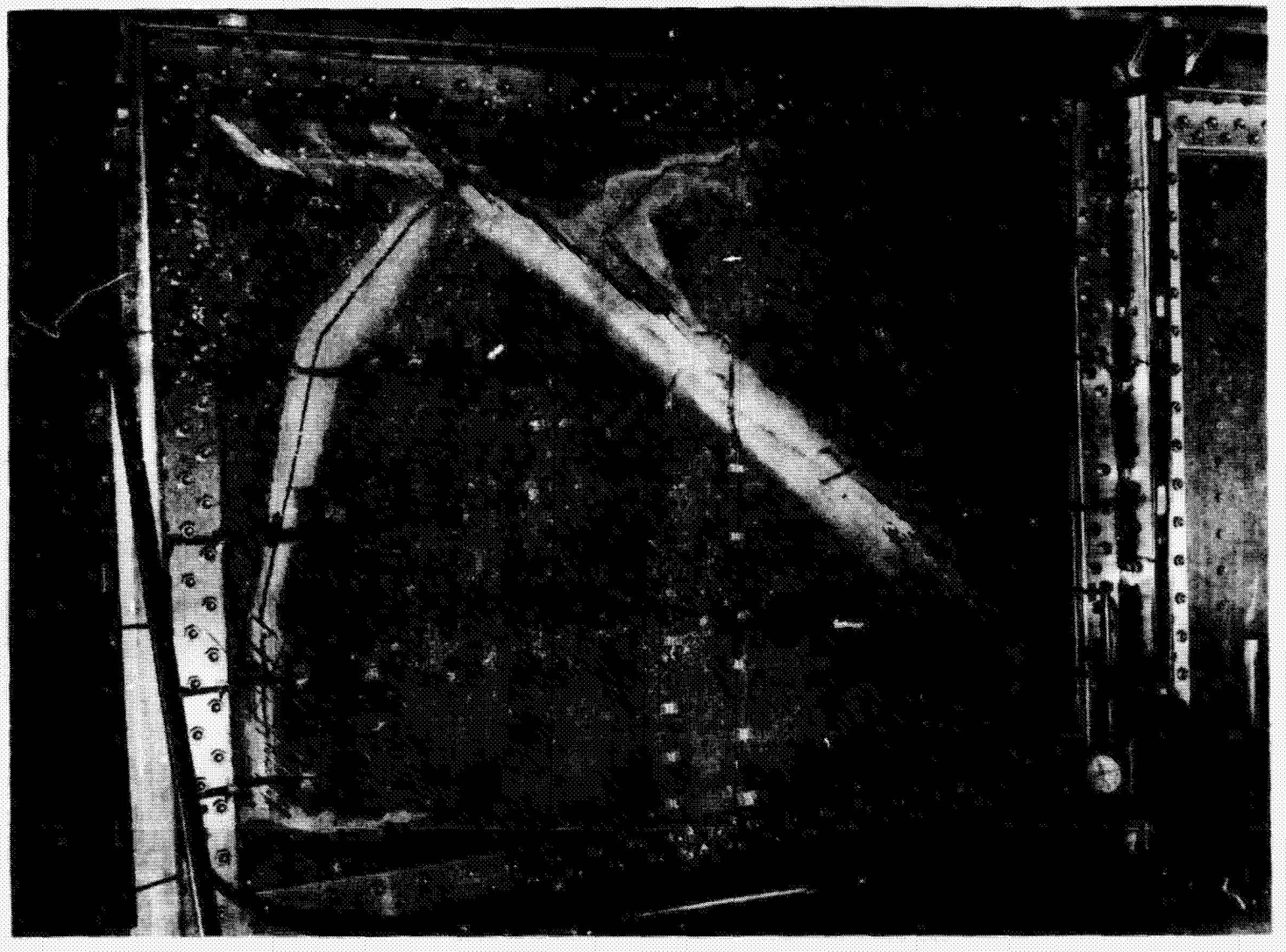

Figure 10(b).- Stability critical shear web after test (Side A).

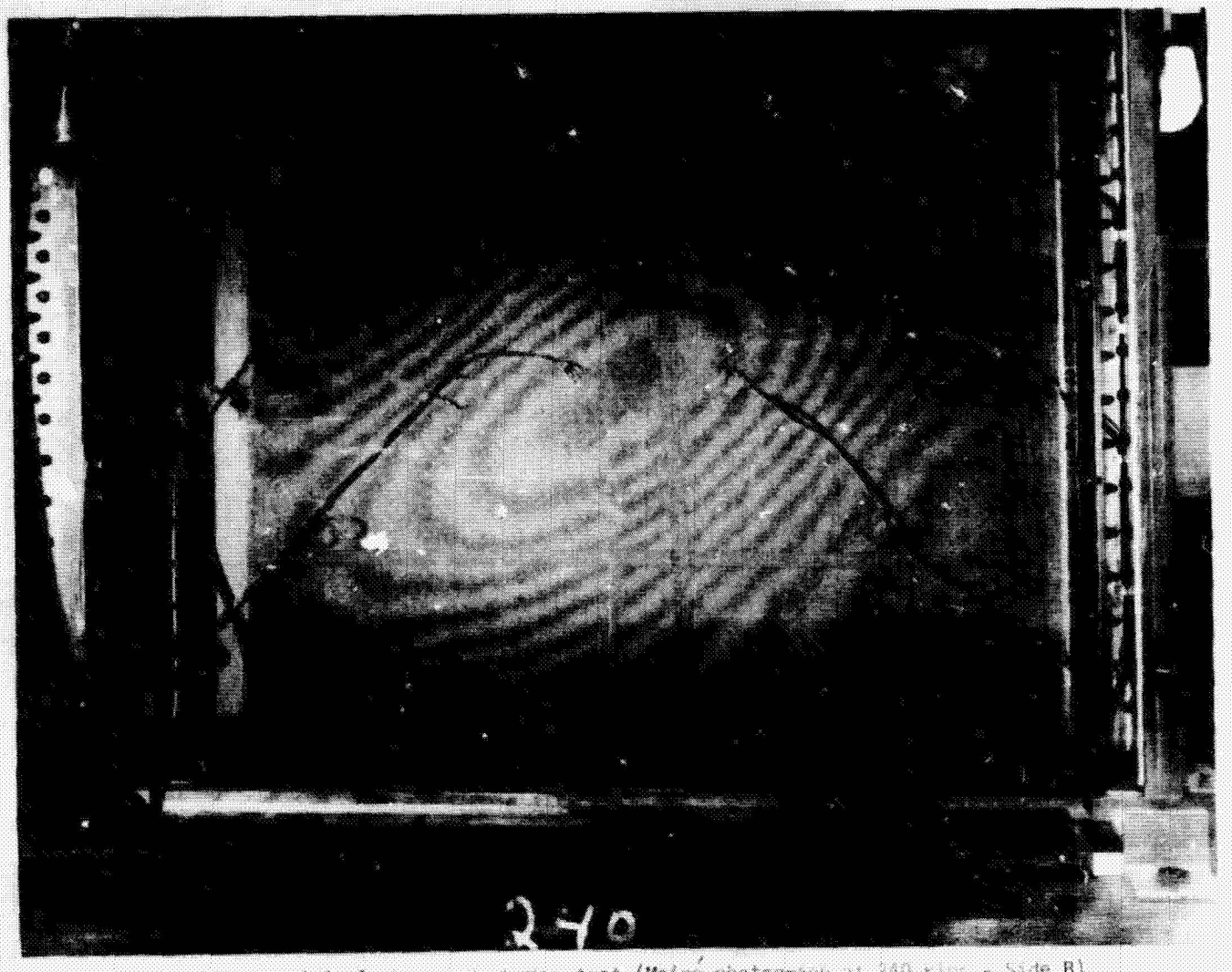

Figure 19.- Stability critical shear web during test (Moiré photograph at 240 kips - Side B).

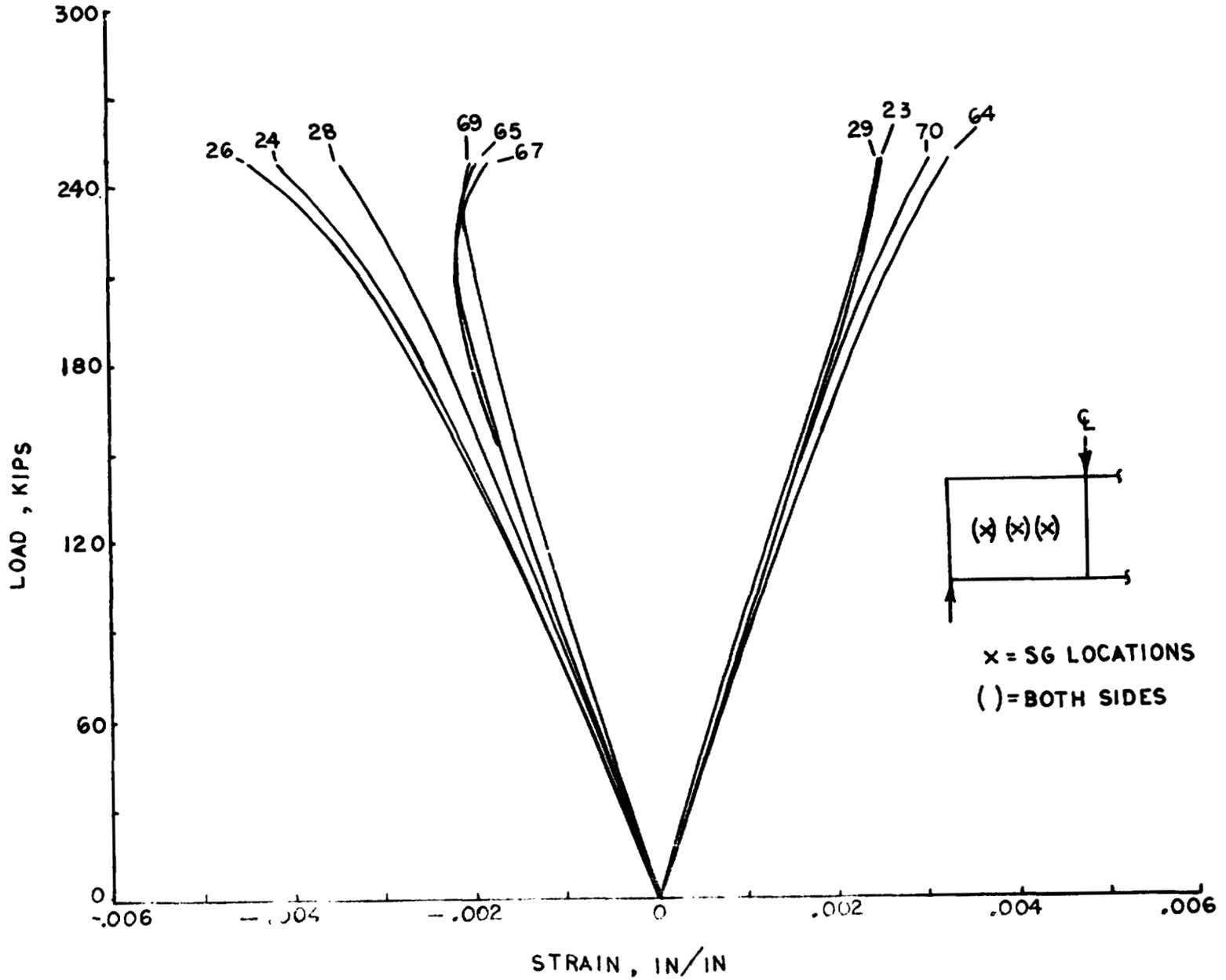

Figure 20.- Stability critical shear web: $\pm$ 45° strains vs load.

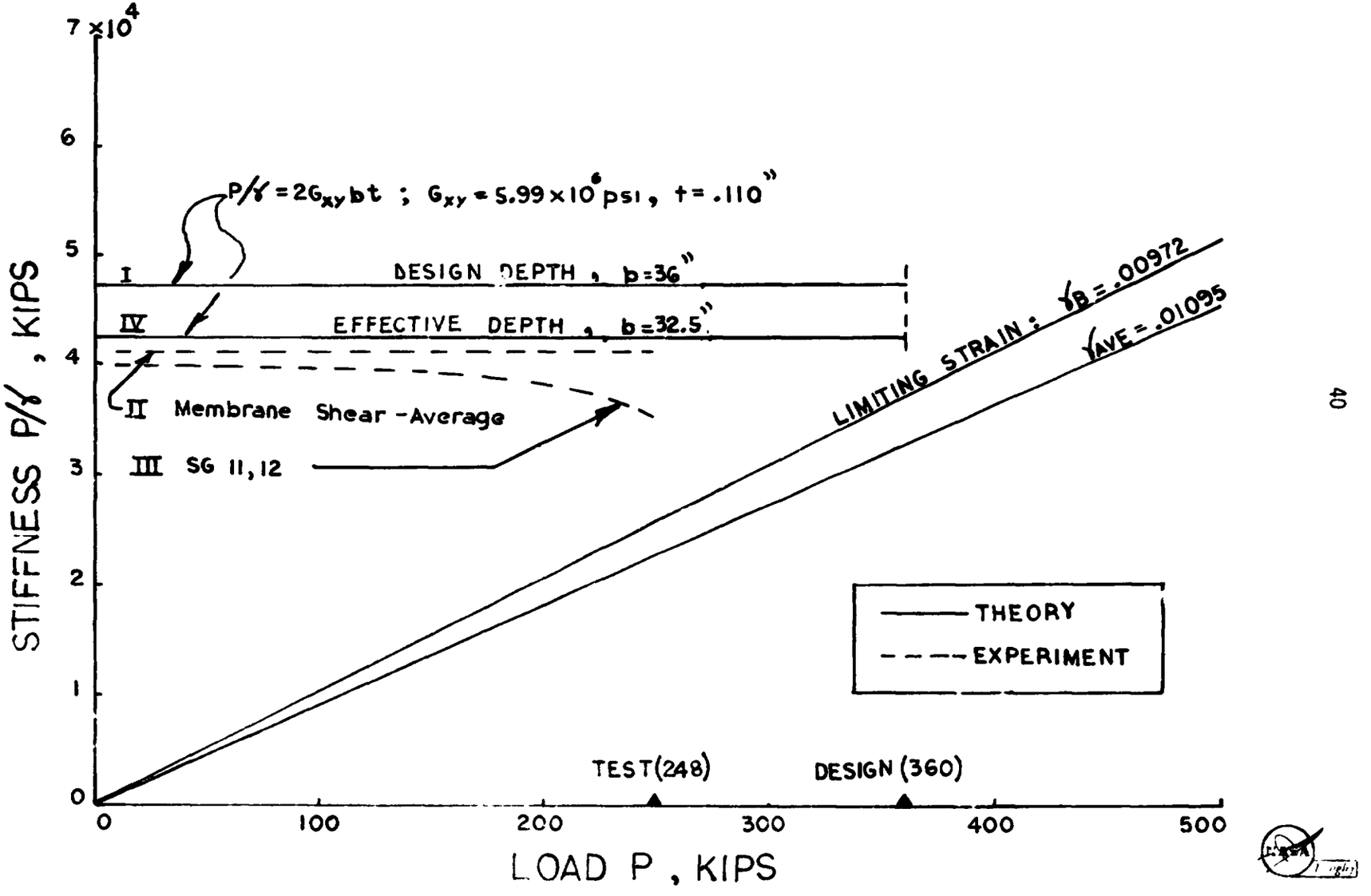

Figure 21.- Force-stiffness plot for stability critical shear web.

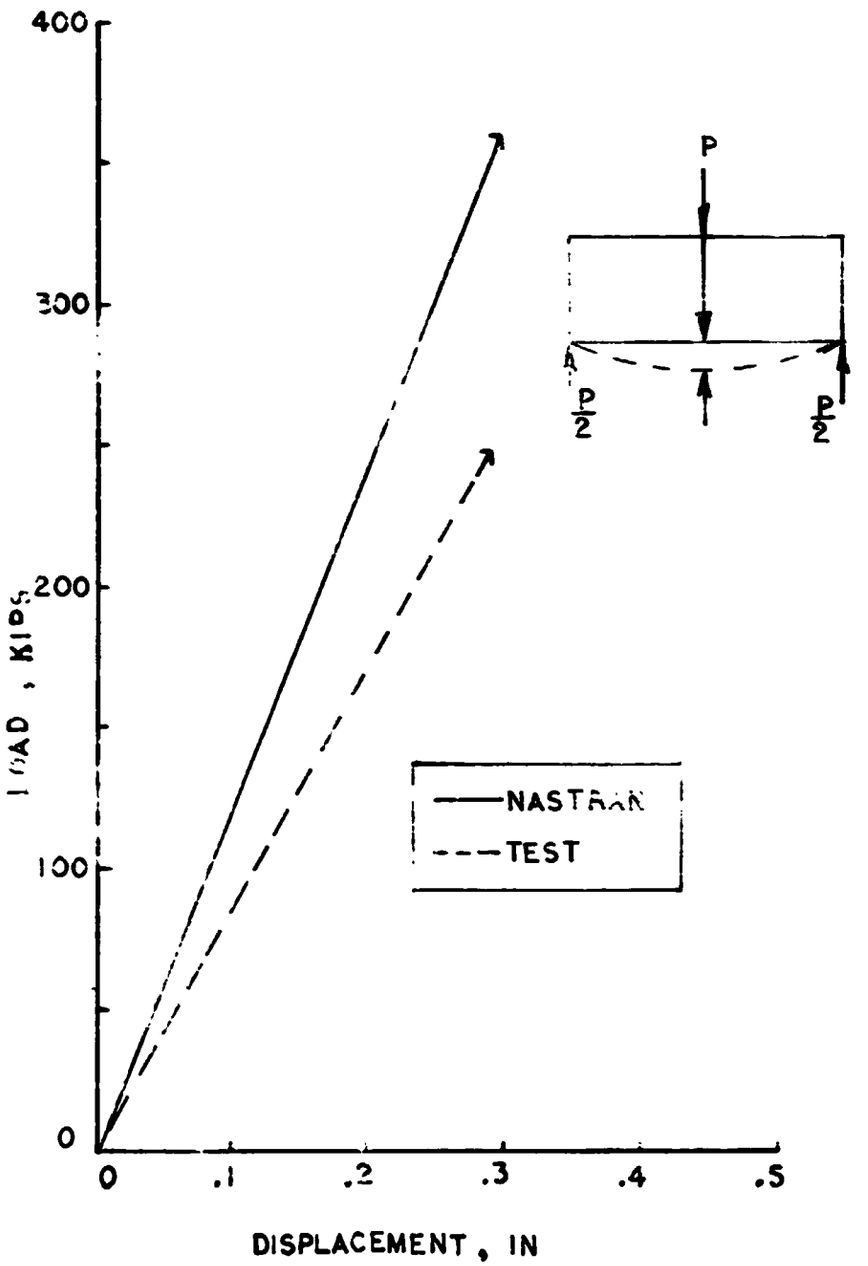

Figure 22.- Vertical displacement at centerline of stability critical web.

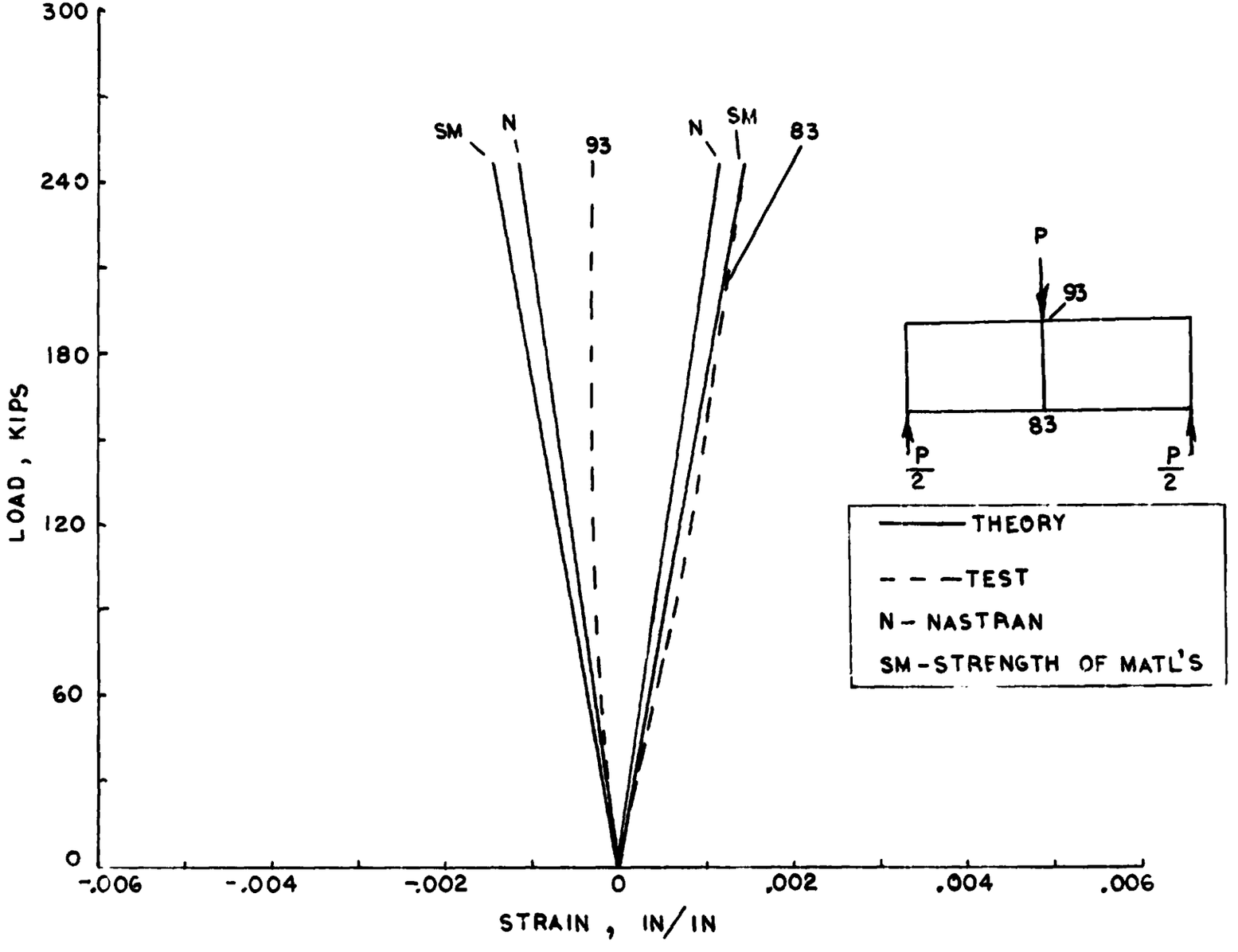

Figure 23.- Cap strains at center of test frame (stability critical web).

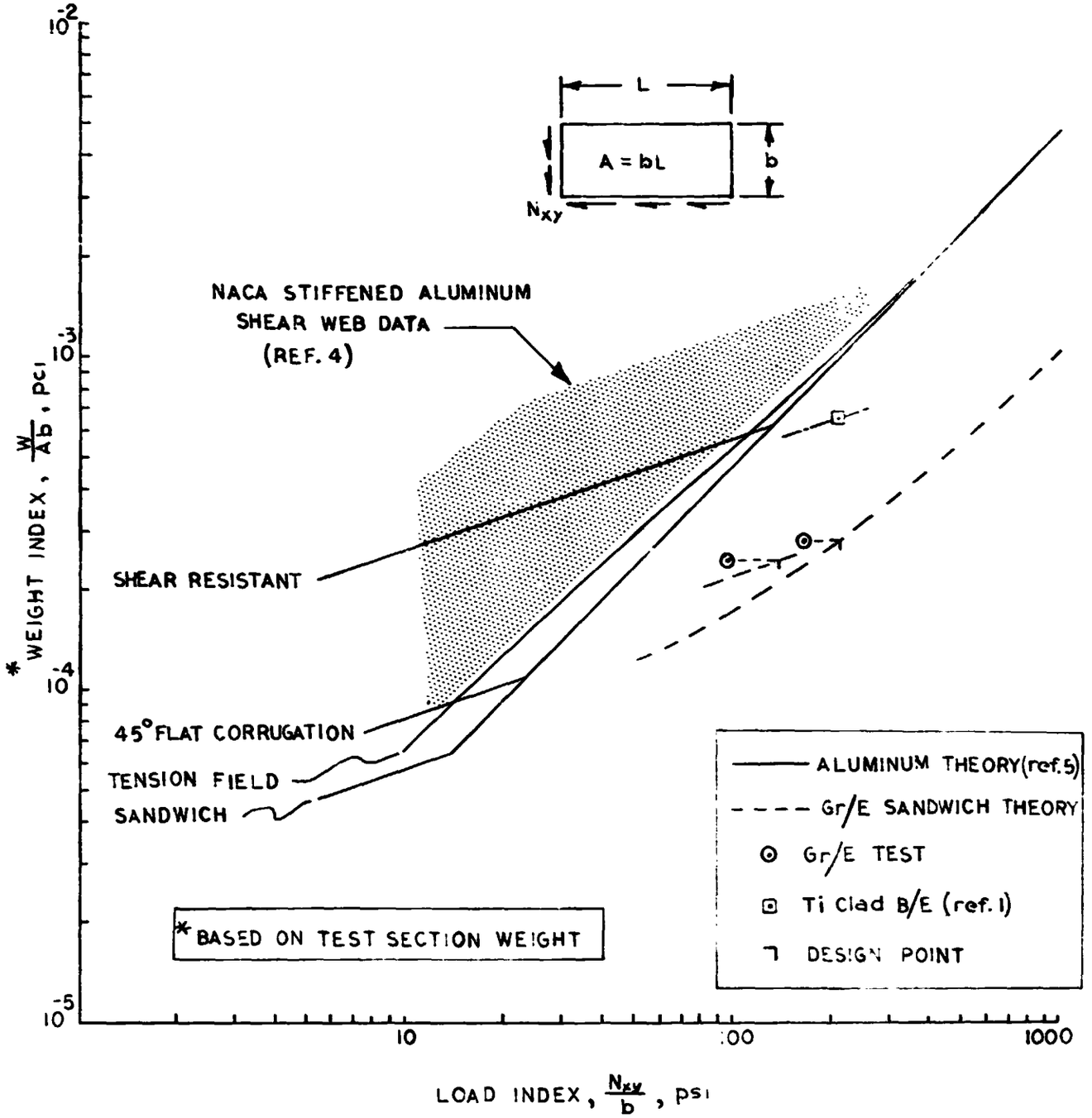

Figure 24.- Shear web weight-strength characteristics.

APPENDIX A

Material Tests

This appendix describes and summarizes the supplementary materials tests which were performed to establish material strength values for design purposes. Also included on test results of sandwich coupons which were taken from the failed shear webs. Tests were performed to investigate laminate strength for (a) shear load, (b) bolt bearing and free hole stress concentrations and (c) compression and tension loading.

Shear tests.- Shear tests of $\pm$ 45° Gr/E (T300/5208) laminate were performed using the biaxially loaded picture frame shown in Figure A1. The sandwich specimen details are shown in figure A2. Five sandwich specimens were tested to failure. The resulting average stress-strain curve is shown in figure A3, along with the failure stress and strain of each specimen. Each individual specimen exhibited linear stress-strain behavior to ultimate load which was characterized by failure perpendicular to the principal tensile stress component direction. The average value of shear strength was 65,560 psi and the average shear modulus was 5.99×10^6 psi. The corresponding "B" value of shear strength was 58,000 psi.

Bolt bearing tests.- The laminate selected for the bolted attachment area of the shear webs was selected to be a $(0/\pm 45/90)$ configuration. Bearing tests were performed to determine the strength of this laminate for design purposes. The specimen configuration used is shown in figure A4. A total of five (5) double-ended specimens were fabricated resulting in ten (10)

tests. These results are presented in Table A1. The average bearing strength was found to be 127,532 psi. The "B" allowable strength was determined to be 116,700 psi.

Open hole tensile tests.- In addition to resisting bolt-bearing in the doubler area of the web. This laminate undergoes both tension or compression due to overall beam bending deformations of the test frame. The stresses due to these inplane deformations are magnified because of the bolt hole (stress concentration effect). To determine the open hole strength of the doubler laminate, ten (10) sandwich beam specimens, detailed in figure A5, were tested with the laminate in tension. The results of these tests are summarized in Table A2.

The average open hole tensile strength was found to be 53,371 psi, and the "B" value was 51,000 psi. A linear interaction between bearing strength and open hole strength was assumed for desig. purposes to size the doubler area thickness.

Compression tests of web sandwich laminate.- To determine the ($\pm$ 45°) Gr/E sandwich web extensional modulus, small (2" x 8") mini-sandwich specimens were cut from undamaged areas of the failed shear panels. Two specimens were cut from each web with the long dimension both parallel and perpendicular to the core ribbon direction to determine if this parameter had any apparent effect on extensional modulus. These specimens were tested in compression. A typical load-strain curve is shown in figure A6. SG-1 & 2 were back to back axial gages and SG 3 & 4 were back to back transverse gages. The specimens were tested to approximately .020 in/in axial strain without failure. There was no discernible effect of core direction on material behavior.

Figures A7 and A8 show typical variations of Poisson's ratio and secant modulus with axial strain. Extrapolating the secant modulus to zero strain yields the initial Young's modulus for the ($\pm$ 45°) material.

This value is seen to be approximately 2.8 x 10^6 which compares well with the modulus value given in Table 2.

Table A1.- Bolt Bearing Strength Test Results for $(0/\pm 45/90)_s$ Laminate - Gr/E (T300/5208)

Test Specimen	Bearing Strength (psi)
1	122,684
2	121,260
3	129,206
4	135,025
5	124.880
6	120,767
7	133,224
8	124,920
9	124,921
10	128,435
σ_{avg} = 127,532 psi σ_B = 116,700	

Table A2 - Open Hole Tensile Strength Test Results for $(0/\pm 45/90)_s$ Laminate - Gr/E (T300/5208)

Test Specimen	Open Hole Tensile Strength (psi)
1	56,146
2	53,233
3	53,472
4	53,164
5	53,456
6	54,317
7	51,873
8	52,707
9	54,620
10	53,326
σ_{avg} = 53,371 σ_B = 51,000	

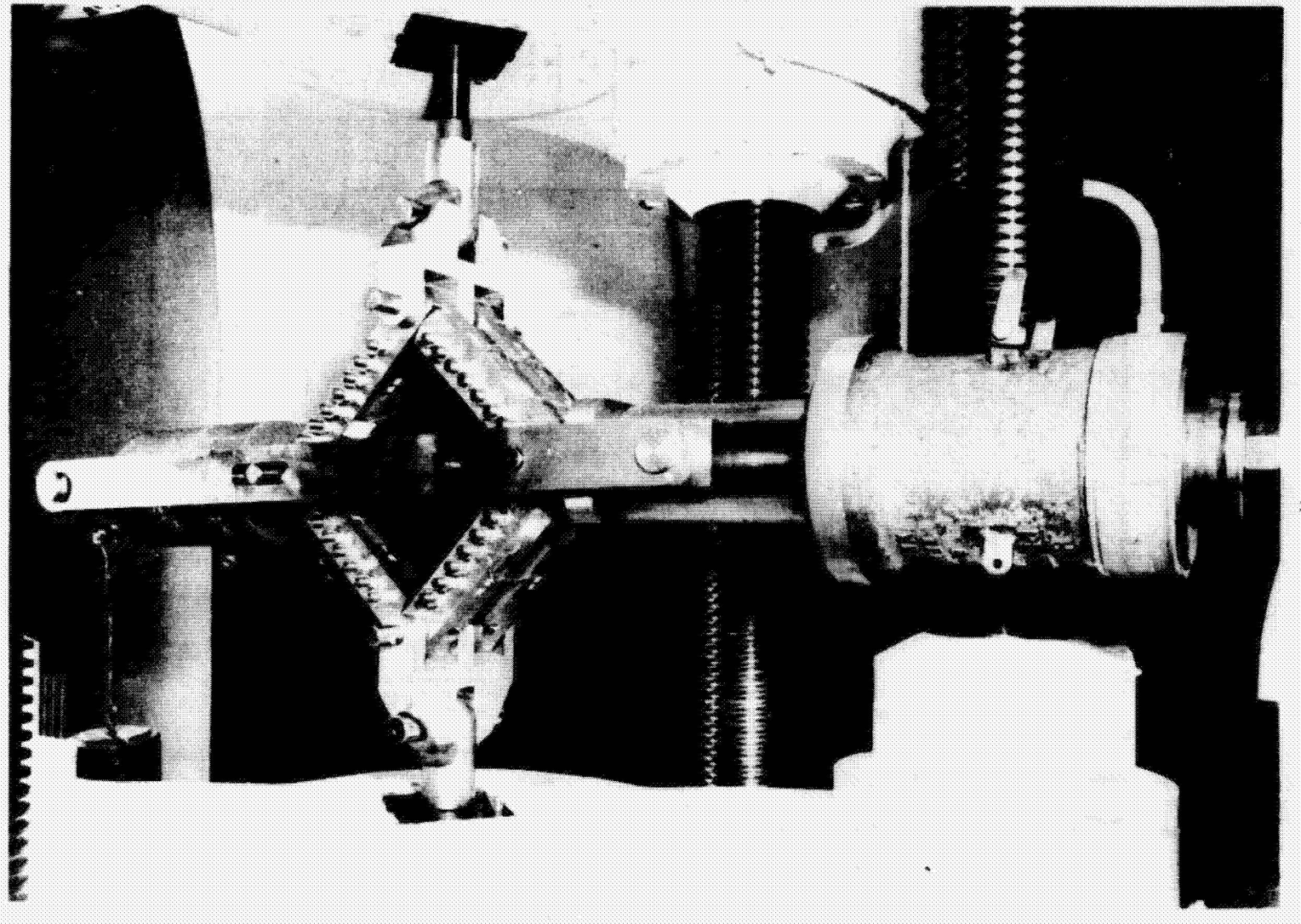

Figure A1.- Biaxially loaded picture frame shear test setup.

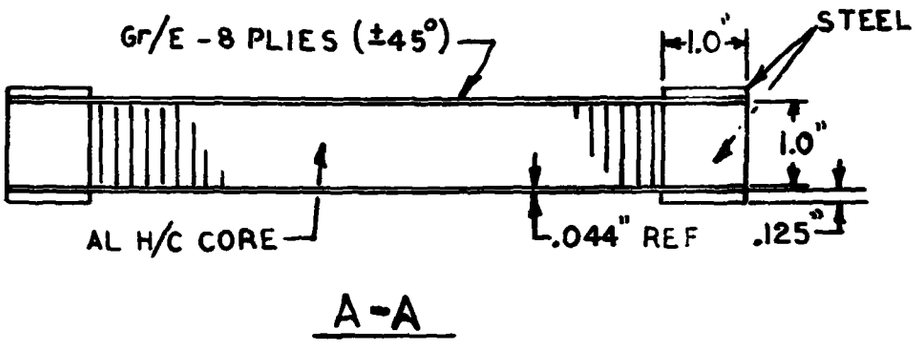

A-A

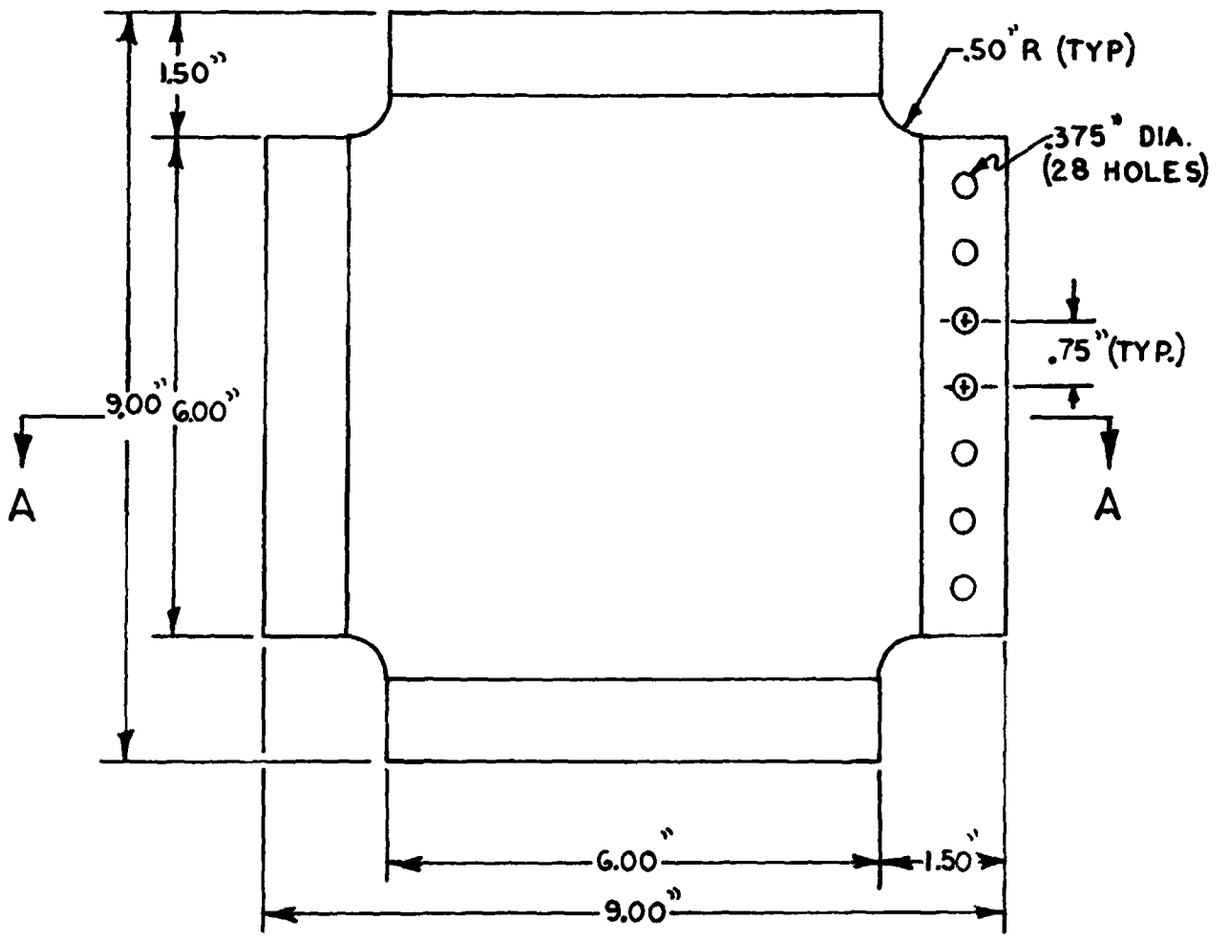

Figure A2.- Shear test specimen configuration.

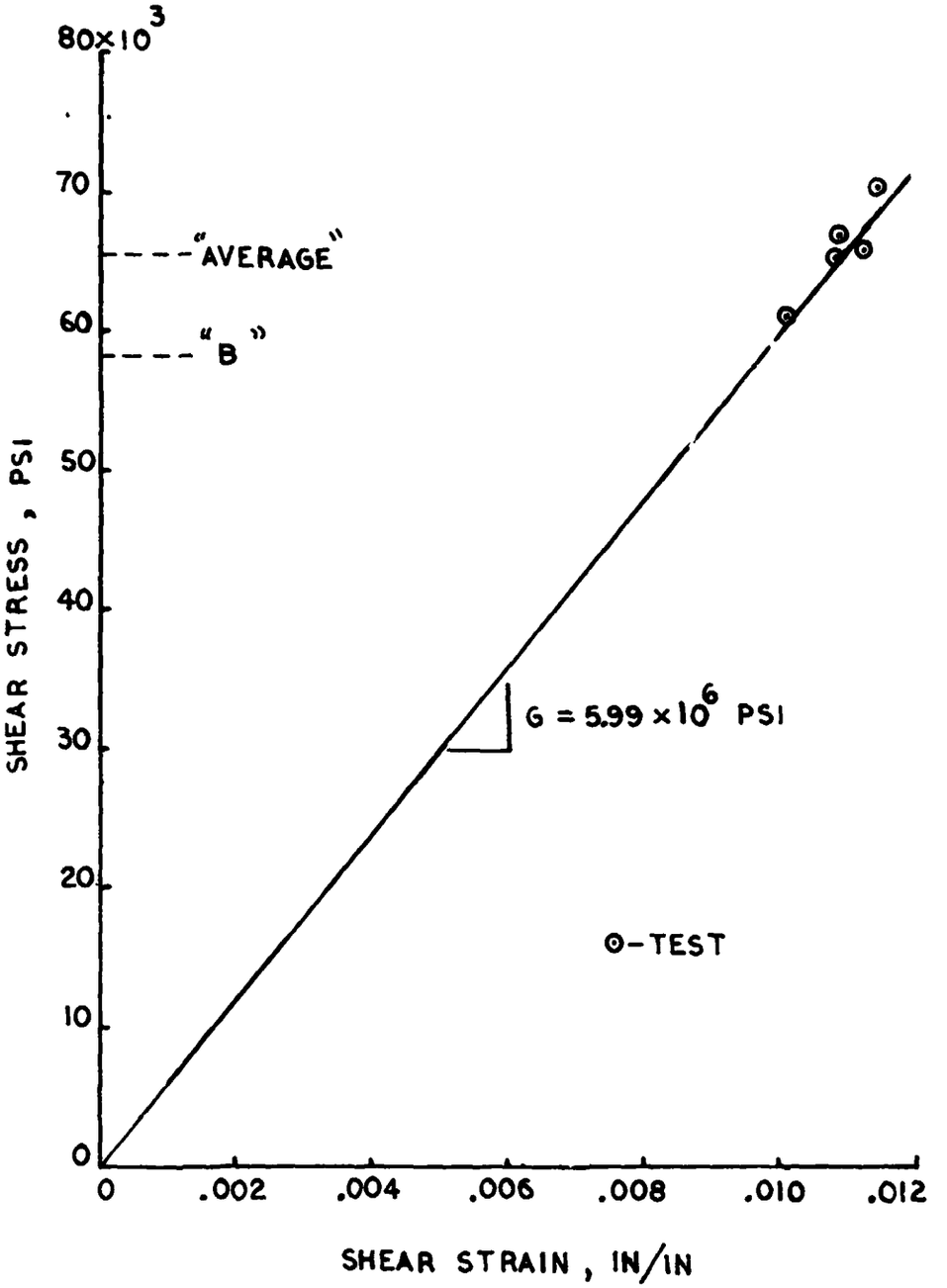

Figure A3.- Inplane shear stress-strain response for (± 45°) Gr/E (T300/5208).

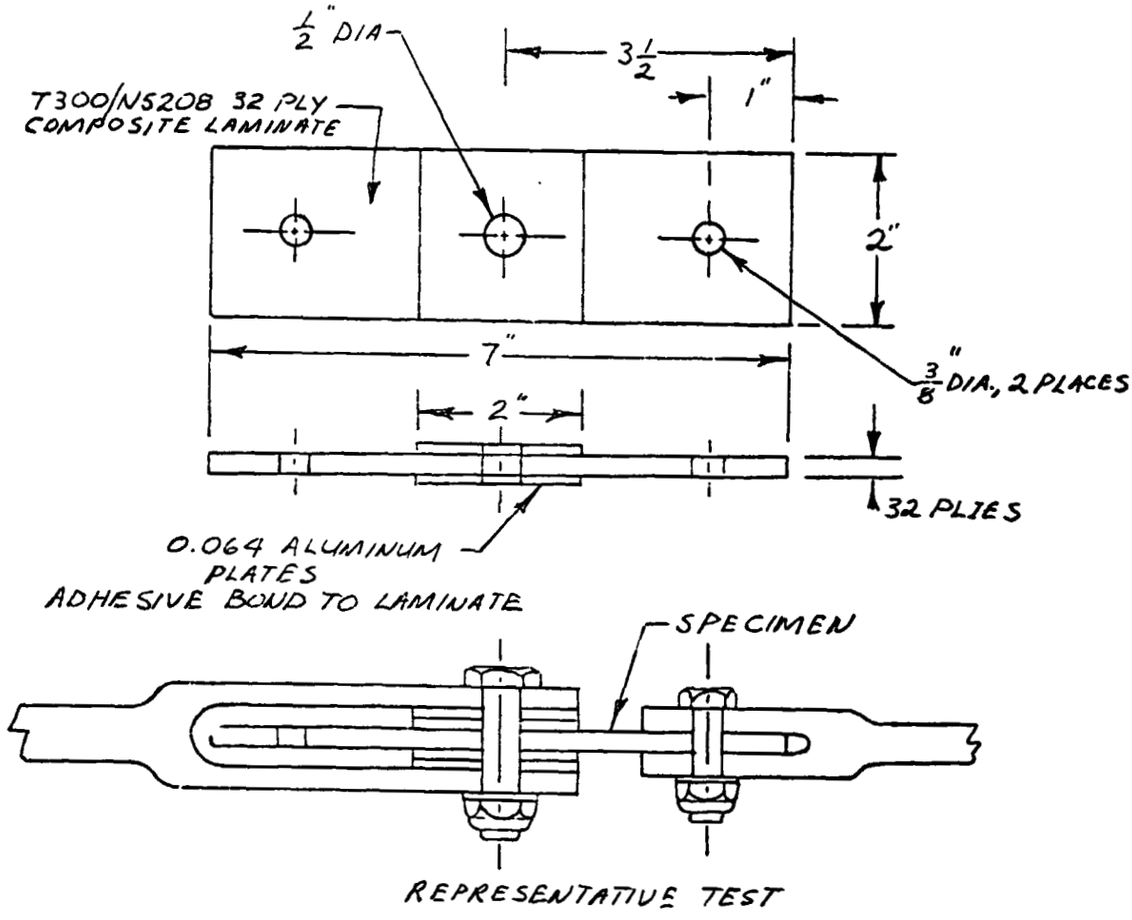

Figure A4.- Double Ended bearing specimen design.

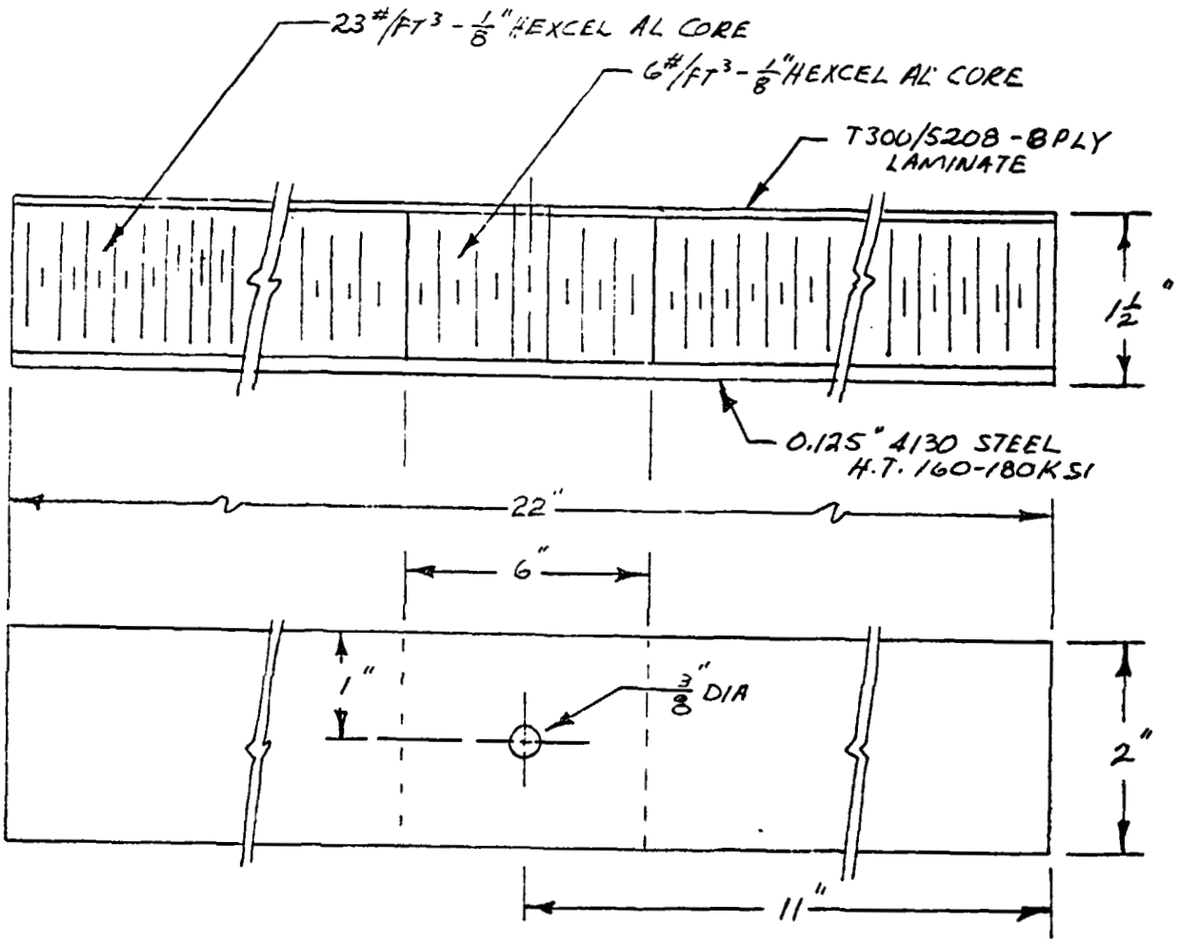

Figure A5.- Open hole sandwich beam specimen design.

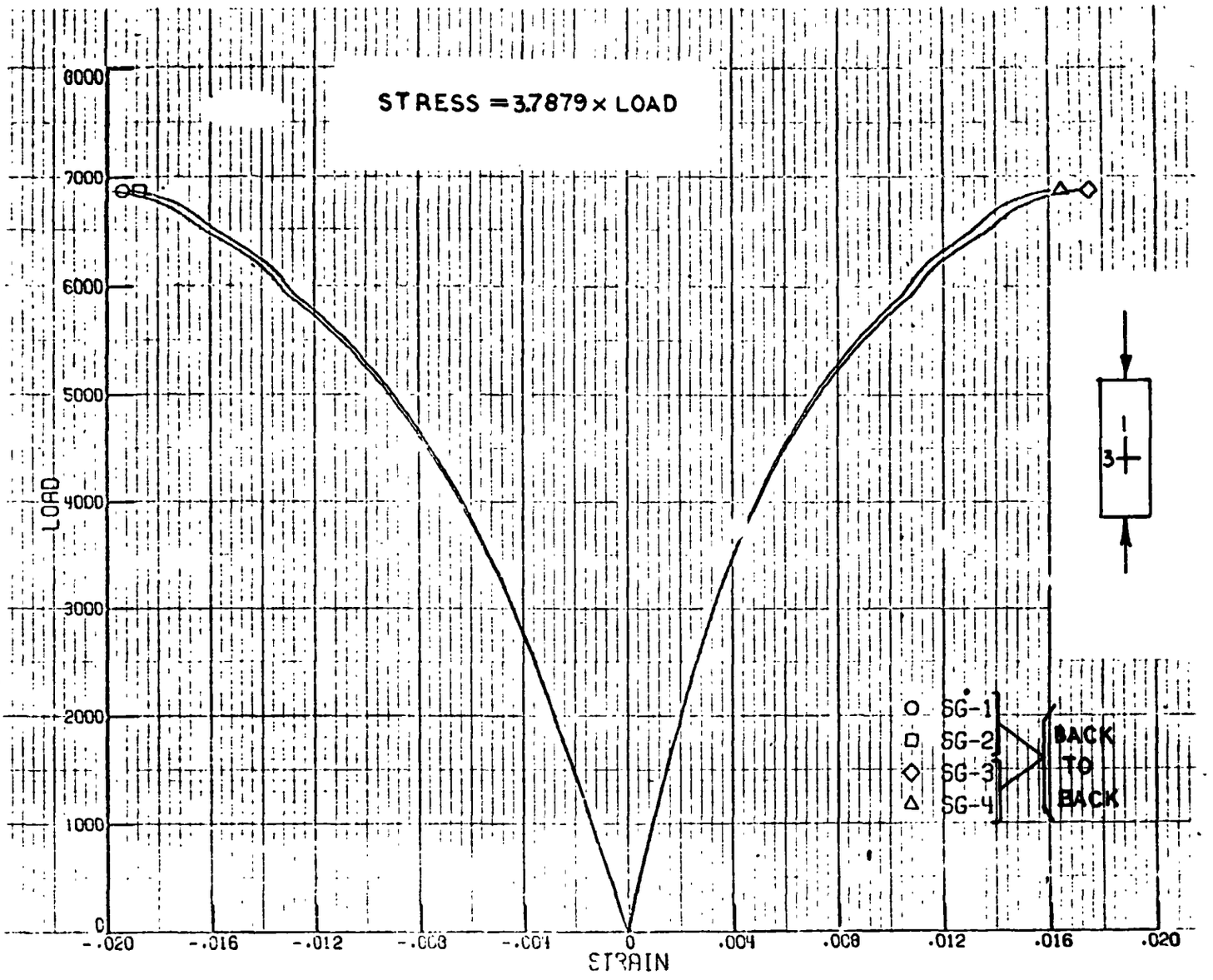

Figure A6.- Typical load-strain response of ($\pm$ 45°) Gr/E T300/5208 laminate.

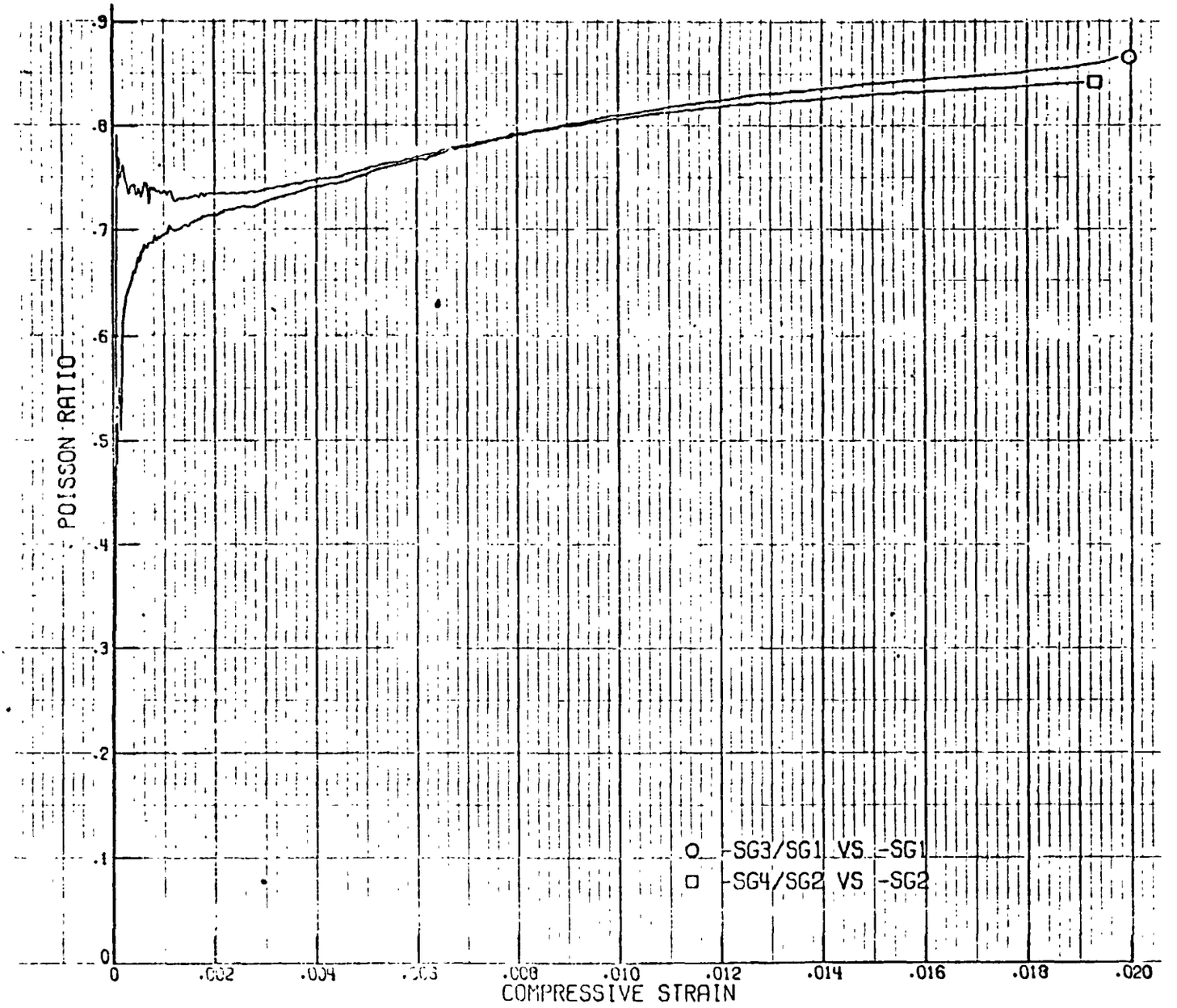

Figure A7.- Typical Poisson ratio variation with compressive strain ($\pm$ 45°) T300/5208.

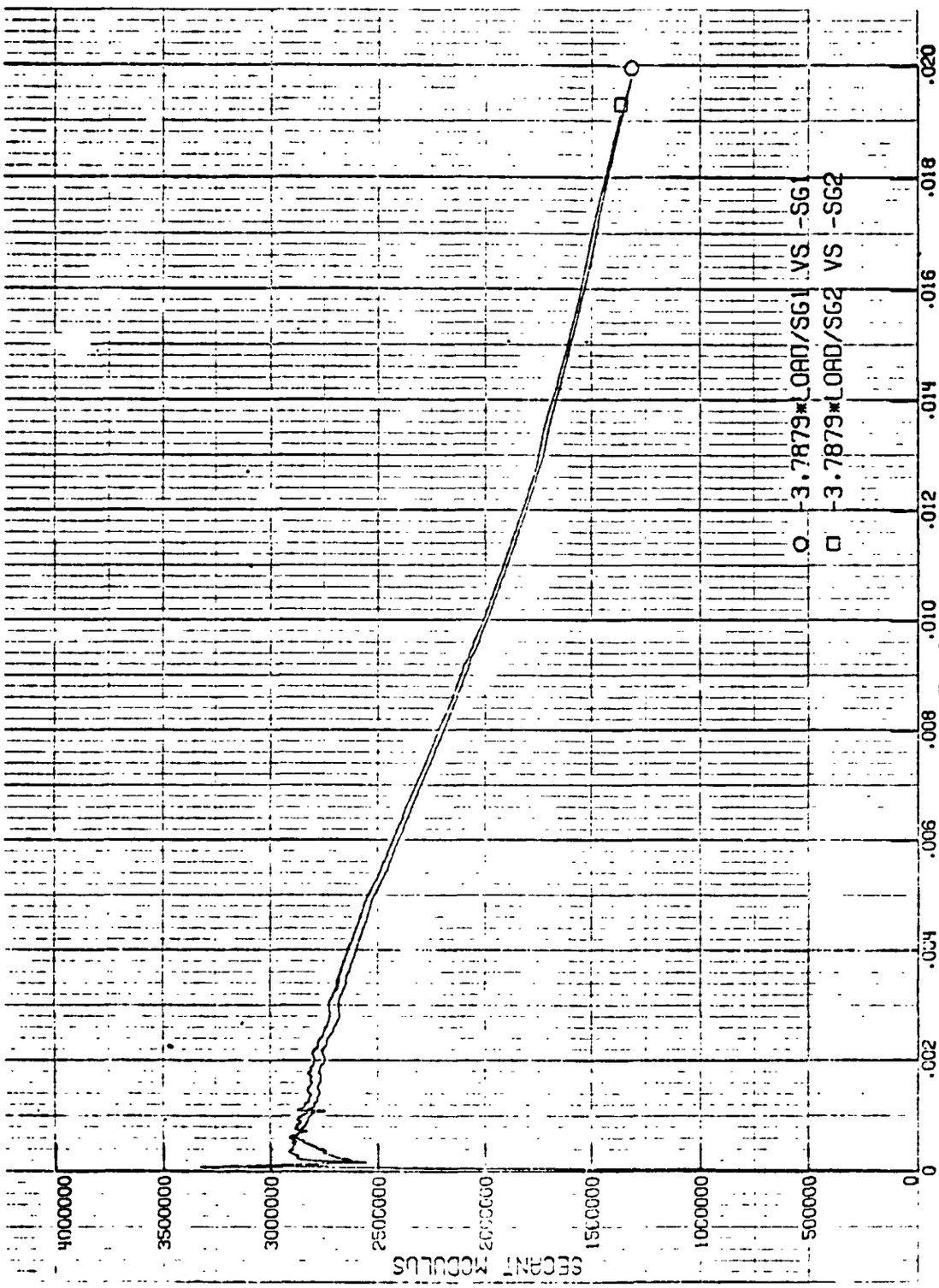

Figure A8.- Typical secant modulus variation with compressive strain- ($\pm$ 45°) 7300/5208.